Since January 2020 Elsevier has created a COVID-19 resource centre with free information in English and Mandarin on the novel coronavirus COVID-19. The COVID-19 resource centre is hosted on Elsevier Connect, the company's public news and information website.

Coordination Chemistry Reviews 427 (2021) 213601

Contents lists available at ScienceDirect

Coordination Chemistry Reviews

journal homepage: www.elsevier.com/locate/ccr

Review

Fluorescent probes based on nucleophilic aromatic substitution reactions for reactive sulfur and selenium species: Recent progress, applications, and design strategies

Yuning Liu [a,b], Yanan Yu [a,b], Qingyu Zhao [a,b], Chaohua Tang [a,b], Huiyan Zhang [a,b], Yuchang Qin [a,b], Xiaohui Feng [a,b,*], Junmin Zhang [a,b,*]

[a] State Key Laboratory of Animal Nutrition, Institute of Animal Science, Chinese Academy of Agricultural Sciences, Beijing 100193, China
[b] Scientific Observing and Experiment Station of Animal Genetic Resources and Nutrition in North China of Ministry of Agriculture and Rural Affairs, Institute of Animal Science, Chinese Academy of Agricultural Sciences, Beijing 100193, China

ARTICLE INFO

Article history:
Received 15 July 2020
Accepted 7 September 2020
Available online 2 October 2020

ABSTRACT

Reactive sulfur species (RSS) and reactive selenium species (RSeS) are important substances for the maintenance of physiological balance. Imbalance of RSS and RSeS is closely related to a series of human diseases, so it is considered to be an important biomarker in early diagnosis, treatment, and stage monitoring. Fast and accurate quantitative analysis of different RSS and RSeS in complex biological systems may promote the development of personalized diagnosis and treatment in the future. One way to explore the physiological function of various types of RSS and RSeS in vivo is to detect them at the molecular level, and one of the most effective methods for this is to use fluorescent probes. Nucleophilic aromatic substitution (S_NAr) reactions are commonly exploited as a detection mechanism for RSS and RSeS in fluorescent probes. In this review, we cover recent progress in fluorescent probes for RSS and RSeS based on S_NAr reactions, and discuss their response mechanisms, properties, and applications. Benzenesulfonate, phenyl-O ether, phenyl-S ether, phenyl-Se ether, 7-nitro-2,1,3-benzoxadiazole (NBD), benzoate, and selenium-nitrogen bonds are all good detection groups. Moreover, based on an integration of different reports, we propose the design and synthesis of RSS- and RSeS-selective probes based on S_NAr reactions, current challenges, and future research directions, considering the selection of active sites, the effect of substituents on the benzene ring, and the introduction of other functional groups.

Contents

* Corresponding authors at: State Key Laboratory of Animal Nutrition, Institute of Animal Science, Chinese Academy of Agricultural Sciences, Beijing 100193, China.
E-mail addresses: fengxiaohui@caas.cn (X. Feng), zhangjunmin@caas.cn (J. Zhang).

https://doi.org/10.1016/j.ccr.2020.213601
0010-8545/

1. Introduction

Reactive sulfur species (RSS) and reactive selenium species (RSeS) are important substances in the redox systems of organisms [1,2]. The former include glutathione (GSH), cysteine (Cys), homocysteine (Hcy), hydrogen sulfide (H_2S), thiophenol (PhSH), polysulfide (H_2S_n), sulfite (SO_3^{2-}), and bisulfite (HSO_3^-) [3–6]. The latter include selenocysteine (Sec), hydrogen selenide (H_2Se), selenite (SeO_3^{2-}), and selenate (SeO_4^{2-}) [7,8]. Proteins containing cysteine or selenocysteine bear thiol or selenol groups, which affect their folding and function [1,9]. The functional sites of some proteins are composed of selenol or thiol groups, such as thioredoxin oxidoreductase (TrxR), selenoprotein P (Seleno P), and glutathione S transferase (GST) [9,10]. These proteins are not only the important part of the redox system of the body, but also facilitate the transport of some important elements, such as sulfur, selenium, and mercury [11–13]. Both sulfur in RSS and selenium in RSeS can adopt a variety of oxidation states ranging from −2 to +4, endowing both classes of species with variable reactivity [10,14,15]. Therefore, RSS and RSeS mediate many redox reactions and physiological processes, offering disease diagnosis and treatment options [16,17]. In recent years, the biology of RSS and RSeS has become a major focus of research.

RSS and RSeS are widespread in cells and organisms, and are the first line of defense of the body's antioxidant barrier [15,17]. Small-molecule thiols and selenols with redox activity are key factors for regulating cell function and body balance by maintaining a steady redox state of the microenvironment and buffering significant redox state changes [2]. Cells have a perfect regulatory system to maintain their redox balance. Abnormal levels of RSS and RSeS result in poor health, reduced immunity, and other factors that may cause various diseases, such as neurodegenerative diseases, cardiovascular diseases, diabetes, muscle diseases, and AIDS in HIV patients [18,19]. PhSH belongs to a class of highly toxic and highly polluting compounds. According to reports, exposure to PhSH in liquid or vapor form can cause a series of serious health problems, including central nervous system damage, impaired breathing, muscle weakness, hind limb paralysis, coma, and even death. It appears that timely suppression and detection of PhSH are very important [3,4].

Aromatic electrophiles are a class of thiol/selenol inhibitors, mainly bearing strongly electron-withdrawing groups (such as nitro, trifluoromethyl, methoxy, etc.) on the benzene ring other than halogens (F, Cl, Br), making it easier for halogens to attack thiol/selenol, forming the corresponding HX (X = F, Cl, Br). At the same time, the Se/S is arylated through a covalent bond to block the thiol/selenol, affecting the function and structure of the protein. 2,4-Dinitrochlorobenzene (CDNB), *p*-nitrochlorobenzene (CNB), *p*-nitrobromobenzene, *p*-methoxychlorobenzene, and *o*-trifluoromethylfluorobenzene are small molecules of this type. Since phenyl itself also has an electron-withdrawing effect, fluorobenzene, chlorobenzene, and so on, can also be used as electrophiles [20–22].

Aromatic small-molecule electrophiles can form a covalent bond with Cys or Sec at the active site of an enzyme to irreversibly inhibit enzyme activity [23]. CDNB and CNB are often used to determine substrate levels of GST [24,25]. This effect of CDNB has also been used in cell culture experiments and animal model experiments. For example, as a depleting agent of GSH, CDNB can be used to monitor the formation of glutathione S-conjugate in the liver and determine its activity. The high proliferation and metabolism of cancer cells makes them produce more reactive oxygen species (ROS) than normal cells. This leads to an imbalance of the redox system in the cell, which in turn leads to oxidative stress [26–28]. In order to combat the harmful effects of ROS and oxidative stress, the content of Trx in the redox system becomes raised [29]. CDNB has the potential to act as an immunostimulant in the treatment of various diseases [30].

With reduced nicotinamide adenine dinucleotide phosphate (NADPH), CDNB can be used as a specific irreversible inhibitor of thioredoxin reductase (TrxR) and improve the activity of NADPH oxidase in the modified enzyme [31]. Without NADPH, CDNB has no effect on TrxR activity, which indicates that CDNB only inhibits the enzyme after blocking the active sites (thiol/selenol) of the reduced TrxR [32–34]. The active site of reduced TrxR is covalently modified by CDNB to produce the corresponding S-aryl derivative, which irreversibly inhibits the activity of the enzyme [35]. TrxR is an important part of the cell redox system [36]. CDNB can induce apoptosis through irreversible inhibition of TrxR activity. Therefore, TrxR is also an attractive target in the design of anticancer drugs [37–41].

The mechanism whereby the aromatic electrophilic compound inactivates the enzyme involves reaction of the active site (thiol/selenol) with the electrophilic inhibitor to form S-C and Se-C bonds [42,43]. Blocking of TrxR by *p*-nitrochlorobenzene and *o*-nitrochlorobenzene may have a positive effect on the removal of ROS. TrxR-SeH blocked by *p*-nitrobenzenesulfonyl chloride or *o*-nitrobenzenesulfonyl chloride will be oxidized by ROS and release the corresponding selenic acid, thus participating in the removal of ROS from the body with the help of GSH [35,36]. Based on the above-mentioned characteristics of aromatic electrophilic compounds, they may also be used as detection groups of fluorescent

Table 1
Summary of S_NAr fluorescence probes specific for RSS and RSeS detection.

Number of Probe	Ex/nm	Em/nm	LOD	Analyte	Application	Response time	Solvent	Reference
1a	460	560	2.0 pM	GSH	Water Sample	10 min	HEPES:EtOH = 99.5:0.5	[135,136]
1b	450	580	2.0 pM	GSH	Water Sample	10 min	HEPES:EtOH = 99.5:0.5	[135,136]
			0.8 pM	Sec	Water Sample	5 min	100% PBS (pH 5.8)	
2	337	520	6.5 μM	Cys	Water sample Milk	27 min	PBS:DMSO = 3:1	[137]
3	530	610	7 μM	Totle biothiols	Living cells	5 min	100% HEPES	[138]
4	490	590	50 nM	Sec	Living cells	10 min	100% PBS	[139]
5	435	585	43.8 nM	H_2S	Living cells	15 min	100% PBS	[140]
6	319	490	180 nM	Cys	Living cells	30 min	PBS:DMSO = 97.5:2.5	[141]
7	370	502	62 nM	Sec	Living cells	3 min	100% PBS	[129]
8	465	555	5 μM	PhSH	Water Sample	5 min	100% PBS	[142]
9	550	593	68 nM	Sec	Living cells	3 min	PBS:CH_3CN = 99:1	[143]
10	635, 730	700, 785	2.95 μM	Sec	Living cells Mice	4 min	Saline:DMSO = 99:1	[144]
11	450	514	23 nM	Sec	Living cells	12 min	PBS:CH_3CN = 98:2	[146]
12	560	706	62 nM	Sec	Living cells	5 min	PBS:DMSO = 1:1	[171]
13	480	534	0.05 nM	H_2S	Living cells	10 min	100% PBS	[172]
14	680	725	40 nM	H_2S	Living cells Mice	20 min	PBS:DMSO = 9:1	[173]
15	452	550	55 nM	H_2S	Living cells zebrafish	5 min	100% PBS	[174]
16	480	535	10 nM	GSH	Living cells	30 min	HEPES:CH_3CN = 4:1	[180]
	390	462	3 nM	Cys		6 min		
17	780	805	330 nM	GSH	Living cells Mice	20 min	HEPES:DMSO = 99:1	[181]
18a	528	588	212 nM	Cys	Living cells	15 min	100% PBS	[151]
19a	470	581	63 nM	Hcy	Living cells	30 min	PBS:CH_3CN = 1:1	[182]
			44 nM	Cys				
19b	525	608	286 nM	Cys	Living cells	90 min	PBS:CH_3CN = 1:1	[182]
20	710	818	20 nM	GSH	Living cells	40 min	100% HEPES	[183]
21	455	546	–	Cys	Living cells	10 min	100% PBS	[185]
	580	622	–	GSH		2 min		
22	488	620	2.6 nM	Cys	Living cells	5 min	100% PBS	[188]
23	520	780	37 nM	H_2S	Living cells Mice	5 min	100% PBS	[189]
24	471	518	27 nM	GSH	Living cells	100 ms	PBS:DMSO = 3:1	[103]
25	582	610	2.5 nM	H_2S	Living cells	20 min	HEPES:Triton X-100:DMSO = 0.01:1:9	[104]
26	470	540, 585	130 nM	Cys	plasma	10 min	100% PBS	[212]
		585	70 nM	GSH				
27	382	455	150 nM	H_2S	Living cells	500 s	PBS:CH_3CN = 99:1	[213]
28	470, 550	546, 609	4.25 μM	Cys	Living cells	12/15 min	PBS:CH_3CN = 4:1	[214]
			5.11 μM	Hcy		20 min		
	550	609	4.30 μM	GSH		20 min		
	410, 550	485, 609	6.74 μM	H_2S		4/20 min		
29	480	540, 630	1.45 μM	Cys	Living cells	10 min	100% PBS	[215]
			1.8 μM	Hcy		20 min		
30	730	796	39.6 nM	H_2S	Living cells	10 min	100% PBS	[219]
31	465	535	–	H_2S	Living cells	30 min	100% PBS	[220]
32	720	640, 785	0.2 μM	Cys	Living cells Mice	5 min	100% HEPES	[229]
33	490	515	71 nM	H_2S_2	Water Sample Living cells	20 min	100% PBS	[230]
34	305	454	44 nM	Cys	Serum	10 min	100% PBS	[232]
			52 nM	Hcy	Living cells			
		587	96 nM	GSH				
35	470	510	82 nM	Cys	Living cells	30 min	PBS:CH_3CN = 11:9	[235]
36	525	550	1.4 nM	GSH	Living cells	30 min	100% PBS	[241]
37a	635	750	1.09 μM	GSH	living cells	3 min	100% PBS	[242]
37b			0.48 μM		tissue samples			
38	400	452	366 nM	Cys	Living cells	15 min	HEPES:CH_3CN = 3:1	[247]
		588	1.07 μM	GSH				
39	543	582	1.14 μM	H_2S	Living cells	60 min	PBS:DMF = 7:3	[248]
	405, 543	374, 582	2.43 μM	Cys				
		374, 432, 582	4.78 μM	Hcy				
		432, 582	2.43 μM	GSH				
40	600	810	26 nM	GSH	Living cells	30 min	100% HEPES	[249]
41	730	736	500 μM	GSH	Living cells Mice	15 min	HEPES:DMSO = 9:1	[250]
42	780	805	630 mM	GSH	Living cells Mice	20 min	HEPES:DMSO = 99:1	[181]
43	620	713	53 nM	H_2S	Living cells	3 min	PBS:CH_3CN = 1:1	[179]

(*continued on next page*)

Table 1 (*continued*)

Number of Probe	Ex/nm	Em/nm	LOD	Analyte	Application	Response time	Solvent	Reference
					Mice			
44	470	525	–	GST	Living cells	10 min	100% PBS	[153]
45–1-a	680	706	280 nM	PhSH	Living cells Mice	30 min	PBS:DMSO = 99:1	[267]
46	447	655	12 nM	PhSH	Water samples Living cells	10 min	HEPES:DMSO = 95:5	[273]
	470	666	10 nM	Sec	Living cells Mice	20 min	100% PBS	[272]
	469	650	80 nM	PhSH	Water Sample Living cells Zebrafish	7 min	PBS:CH_3CN = 4:1	[274]
47	455	658	3.4 nM	PhSH	Water samples	160 s	PBS:DMSO = 4:1	[275]
	455	666	6 nM	H_2S	Living cells Mice	1 min	HEPES:DMSO = 4:1	[276]
48	523	644	53 nM	S^{2-}	Living cells	30 min	100% PBS	[278]
49				H_2S		Very slow		[270]
50	550	676	29 nM	PhSH	Water samples Living cells	8 min	PBS:DMSO = 1:1	[277]
51	482	655	43 nM	H_2S_n	Living cells	24 min	PBS:DMSO:Tween 80 = 96.6:3:0.4	[271]
52	440	543	51 nM	Cys	Living cells	2 min	HEPES: Ethanol = 1:2	[279]
		543	16 nM	Hcy		2 min		
		583	34 nM	GSH		2 min		
53	440	670	30 μM	H_2S	Living cells	15 min	PBS:DMSO = 7:3	[280]
54-S-1	440	540	35 nM	Cys	Living cells	30 min	PBS:CH_3CN = 7:3	[154]
		547	46 nM	GSH				
		543	50 nM	Hcy				
54-O-6	440	493	41 nM,	Cys	Living cells	30 min	PBS:CH_3CN = 7:3	[154]
			47 nM	GSH				
			65 nM	Hcy				
55	445	560	3.7 nM	GST	Living cells	30 min	100% HEPES	[155]

probes based on S_NAr reaction, applicable for the detection of RSS and RSeS in vitro, in cells, and in animals.

Fluorimetry is a simple, inexpensive, and fast method for detecting analytes. The rise of the rapid detection field in recent years has provided broad scope for the development of fluorimetry [44–48]. In 2014, China formulated the "Proposal for Management of On-Site Rapid Testing (POCT) in Medical Institutions (In Hospitals)", and in 2015 the rapid testing method was written into the Food Safety Law of the People's Republic of China and rapid testing was further recognized [49,50]. In early 2020, large-scale outbreaks of a new coronavirus (2019-nCoV) led to an urgent need for rapid detection methods. Indeed, this became one of the most widely reported and urgent needs for rapid detection [51].

Fluorescent probes have been widely studied and applied in many fields. In particular, their capacity to be used in temporal and spatial sampling and in vivo imaging applications makes them suitable for monitoring physiological and pathological processes, and they have continued to attract ever more attention in biomedical research [52–56]. By modifying the fluorescent matrix, a fluorescent probe can provide dynamic information about the location and quantity of an analyte in different matrices, so that the analyte can be easily studied [57–59]. Fluorescent probes can be used to remotely measure analytes and can be used in environments and samples that are difficult to access directly to avoid possible damage when the analyte is taken out of its natural medium. Fluorescent probes have become important tools in chemical and

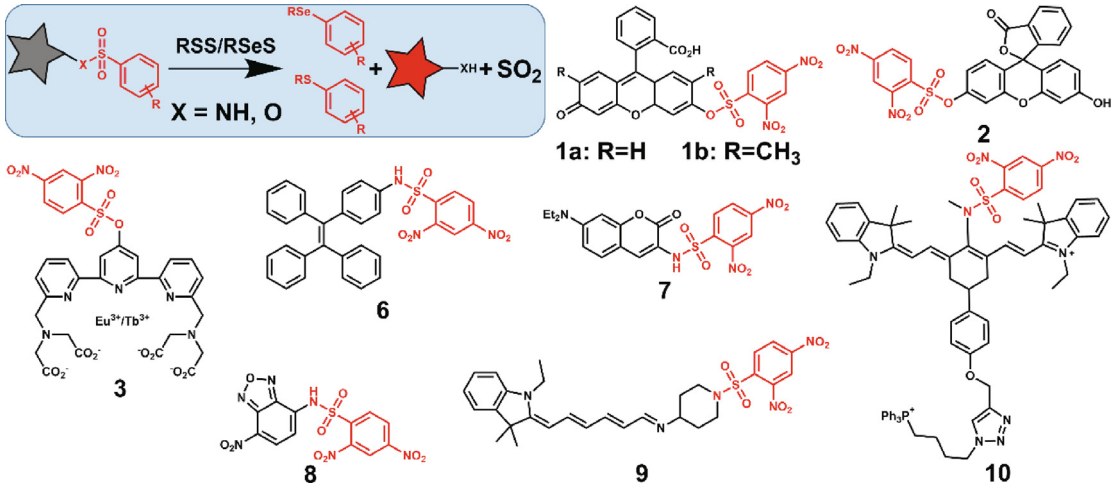

Fig. 1. Benzenesulfonyl-based RSS/RSeS-specific fluorescent probes and their detection mechanisms.

biochemical research due to their non-invasiveness, high sensitivity, high selectivity, operability, low cost, rapid response, high time resolution, and appropriate beneficial characteristics for easy signal detection [60–65].

RSS- and RSeS-specific fluorescent probes have long been used for protein labeling [37,66–68]. For the purpose of drug simulation and structural screening, researchers have synthesized various RSS-specific fluorescent probes [69]. At the beginning of the 21st century, researchers synthesized various types of highly selective RSeS-specific fluorescent probes capable of operating under physiological conditions by simulating the structure of RSS probes and optimizing the detection environment. Fluorescent probes based on S_NAr reaction for RSS and RSeS have been hot spots in this field [7,8,66].

Because RSS and RSeS are prone to deprotonation, and their amounts in vivo are very small, the development of RSS- and RSeS-specific fluorescent probes for intracellular or in vivo targeting is very challenging [7,8]. Observing the endogenous or exogenous RSS and RSeS in cells or animals is an important application of fluorescent probes [67,70–72]. RSS- and RSeS-specific fluorescent probes should be able to provide insight into changes in specific RSS and RSeS in healthy and diseased cells and biological systems [73–75]. For the differentiation of different types of proteins containing Cys or Sec, as well as the detection of RSS and RSeS in blood, tissue, agricultural products, and food, the effect of thiols on food flavor is worth exploring [76–79]. In this review, we first briefly summarize the latest developments in the field of fluorescent probes for RSS and RSeS based on S_NAr reactions. Thereafter, based on the integration of different reports, we propose methods for the design and synthesis of RSS- and RSeS-selective probes based on S_NAr reactions, current challenges, and future research directions, considering the selection of active sites, the effect of substituents on the benzene ring, and the introduction of other functional groups.

2. Fluorescent probes for RSS and RSeS based on S_NAr reactions

The reaction of an electrophilic aromatic compound and a fluorophore can have a strong quenching effect on the probe [3,4]. Most fluorescent probes based on S_NAr reactions for RSS and RSeS can achieve the "off–on" effect after reaction with the analyte [7,8]. Benzenesulfonate [80–88], phenyl-O ether [89–98], phenyl-S ether [99–102], phenyl-Se ether [103,104], 7-nitro-2,1,3-benzoxadiazole (NBD) [105–111], benzoate, and selenium-nitrogen bonds are all good detection groups [21,22] (see Table 1).

2.1. Benzenesulfonic acid as the detection group

Benzenesulfonamide and benzenesulfonate are the main reactive groups of benzenesulfonic acid [20,112–120]. RSS and RSeS can break the benzenesulfonamide or benzenesulfonate bond and become bound to the aromatic part of the detection group with the concomitant release of SO_2. Due to the extinction of the quenching group, the fluorescence is enhanced, thus providing the test signal [121–128]. Compared with the benzenesulfonate bond, the p-π conjugation effect of the benzenesulfonamide bond makes it stronger and more difficult to break, so it is more suitable to detect RSS with lower pK_a values in a physiological environment, such as H_2S, PhSH, and even Sec [129–134].

Hatsuo et al. have long been engaged in research on fluorescent probes for thiols. They appended 2,4-dinitrobenzenesulfonyl to rhodamine, and thereby synthesized two fluorescent probes (Fig. 1, panels **1a** and **1b**) that could be used for thiol detection at physiological pH [135,136]. The reaction rates of probes **1a** and **1b** with GSH were 1.7×10^2 and 1.4×10^2 M^{-1} s^{-1}, respectively, and the detection limits for GSH and Cys were both lower than 2.0 pM, making these probes suitable as substitutes for the Ellman reagent in the quantitative determination of thiols. In further studies, Hatsuo et al. found that probe **1b**, which was originally designed to detect thiols, reacted more quickly with selenols in phosphate buffer at pH 5.8, with an emission intensity ratio (I_{SeH}/I_{SH}) exceeding 200 [136]. The rate of reaction of this probe with Sec was 7.4×10^2 M^{-1} s^{-1} and the detection limit was 0.8 pM. However, this measurement method is incompatible with biological environments.

Although many fluorescent probes have been used to detect Cys, most of them have been used to image living cells, and detection methods based on fluorescent probes for Cys in foods need further development. Yang et al. appended a 2,4-dinitrobenzenesulfonyl moiety to fluorescein and applied the synthetic probe (Fig. 1, panel **2**) to the detection of Cys in milk and water samples [137]. The probe proved to be highly selective and could be used to detect Cys concentrations in the range 0–400 μM. Its excitation and emission wavelengths of λ_{ex} = 337 nm and λ_{em} = 520 nm were not affected in the range pH 6–9, the detection limit was 6.5 μM, the color of the solution changed from light-yellow to yellow-green, and the detection of Cys using this probe could be recognized by the naked eye.

(4′-Hydroxy-2,2′:6′,2″-terpyridine-6,6″-diyl)-bis(methyleneni trilo)tetrakis(acetic acid) (HTTA) is a functional ligand that can form highly stable complexes with both Eu^{3+} and Tb^{3+} ions. Yuan et al. found that the terbium(III) complex of this ligand (HTTA-Tb^{3+}) has a higher fluorescence quantum yield under physiological conditions. However, its europium(III) complex (HTTA-Eu^{3+}) has only weak fluorescence due to the negative charge on oxygen (terpyridine-O^-) after deprotonation of the hydroxyl group on terpyridine. By introducing a 2,4-dinitrobenzenesulfonyl (DNBS) group on the HTTA structure, a ratio-based fluorescent probe (Fig. 1, panel **3**) for biothiols was synthesized [138]. Due to the occurrence of photoinduced electron transfer (PET), NSTTA-Eu^{3+} and NSTTA-Tb^{3+} showed weak fluorescence. However, when reacted with a thiol, due to departure of the DNBS group, the PET function was lost, making the fluorescence of the terbium(III) complex significantly enhanced, whereas the fluorescence intensity of the europium(III) complex did not change significantly. Therefore, the fluorescence intensity ratio of the terbium(III) complex to the europium(III) complex (I_{540}/I_{610}) could be used as a fluorescence marker to perform quantitative detection of thiols. Indeed, it has been used for ratiometric imaging of thiols in several cell samples. NSTTA-Tb^{3+}/Eu^{3+} was used to detect thiols in 5 min with a detection limit of 7 μM.

Xu et al. have been studying polymer micelles for a long time, using ring-opening polymerization (ROP) of cyclic carbonates to synthesize amphiphilic polymers. Through modification with 2,4-dinitrobenzenesulfonyl moieties, they synthesized a fluorescent derivative of the drug doxorubicin (DOX) and polycarbonate micelles (PMPC-DNS) capable of responding to Sec (Fig. 2, panel **4**) [139]. The amphiphilic copolymer could self-assemble to give a hydrophobic core with a hydrophilic shell at the periphery. It is worth noting that the hydrophobic termini of the micelle are the recognition sites for Sec. In the presence of Sec, the 2,4-dinitrobenzenesulfonyl recognition site is activated, rendering it hydrophilic and destabilizing the micelle, thereby releasing DOX. In this way, Sec can be detected in cells and tissue. PMPC-DNS formed spherical micelles with an average diameter of 118 nm in aqueous solution. The critical micelle concentration (CMC) was determined as 0.01245 mg mL^{-1}. The drug loading efficiency (DLE) and drug loading content (DLC) of the micelle for DOX were 6.5% and 7.63%, respectively. The PMPC-DNS probe was successfully applied for the imaging of endogenous Sec in HeLa cells and live cervical tumors.

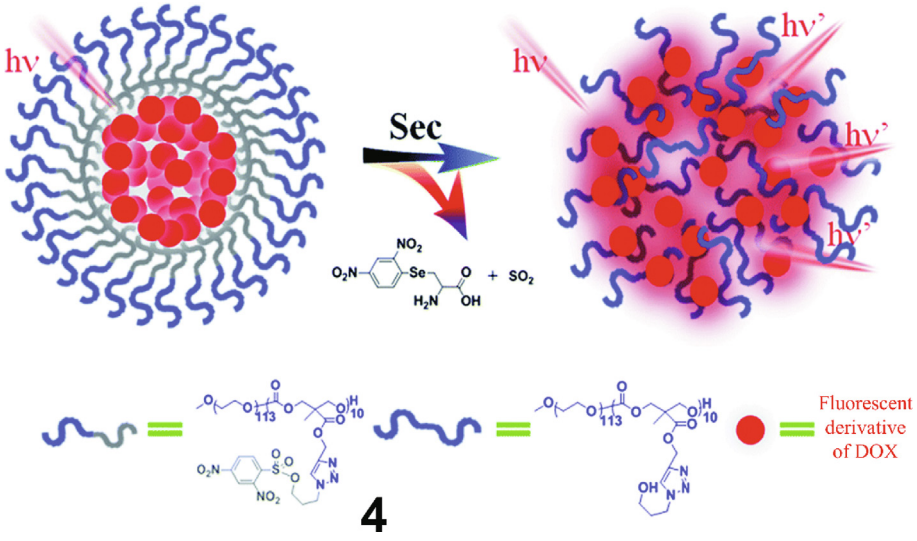

Fig. 2. Strategy for detection of Sec by probe 5 [139].

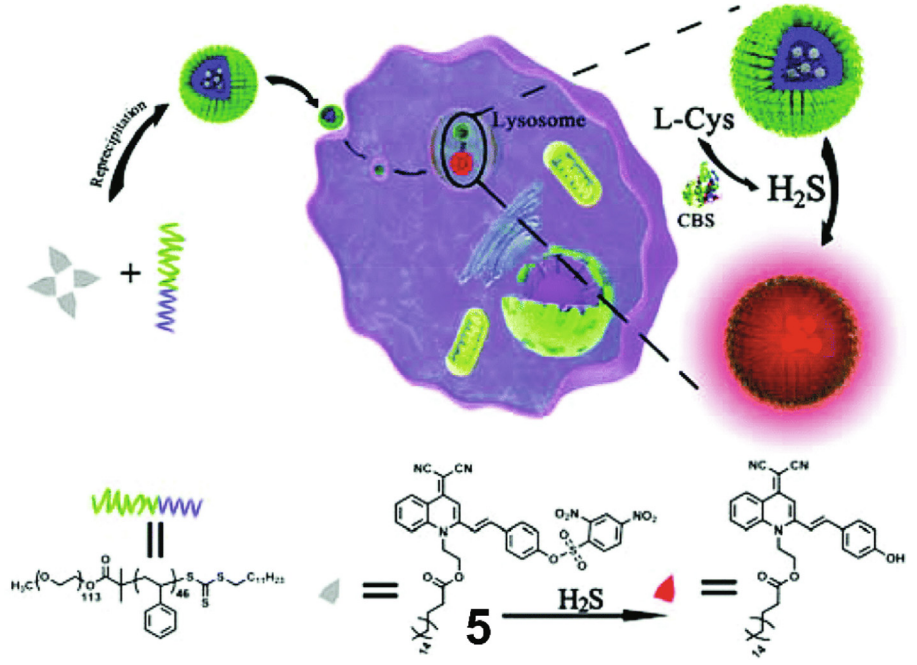

Fig. 3. Strategy for detection of H_2S by probe 6 [140].

Aggregation-induced emission dots (AIED) have various advantages, such as high fluorescence, large Stokes shift, excellent light stability, and good biocompatibility. Gao et al. developed a new type of nanoprobe based on AIED for selective monitoring of endogenous H_2S levels in lysosomes (Fig. 3, panel **5**) [140]. The prepared AIED showed good water dispersibility, optical parameters of λ_{ex} = 435 nm and λ_{em} = 585 nm, a detection limit of 43.8 nM, selectivity for H_2S superior to that of other thiols, and excellent long-term stability (>16 weeks). In addition, confocal fluorescence imaging experiments confirmed that AIED mainly resided in lysosomes, permitting specific imaging of the levels of exogenous and endogenous H_2S in living cells.

Based on the simple synthesis of tetrastyrene (TPE), easy modification, and the special properties of aggregation-induced emission (AIE), Li et al. designed and synthesized a tetrastyrene-based fluorescent probe $TPENNO_2$ for the specific detection of Cys (Fig. 1, panel **6**) [141]. The kinetic rates of reactions of this probe with Cys, Hcy, and GSH, respectively, were determined. It was found that the changes in their fluorescence responses with time were different. Thus, Cys, Hcy, and GSH could be detected sequentially according to different time sequences. The response time of this probe to cysteine was 30 min, the detection range was 0–500 μM, with λ_{ex} = 319 nm and λ_{em} = 490 nm, and the limit of detection was 0.18 μM. In addition, $TPENNO_2$ could also be used for the detection of thiols in live cells.

Fang et al. constructed a small library of selenol probes based on the mechanism of S_NAr. By adjusting the reactivity of the probes, a fluorescent probe (Sel-green) with high selectivity for selenol under physiological conditions was identified, and the relationship between the probe structure and activity was established (Fig. 1,

panel **7**) [129]. 2,4-Dinitrophenyl is a strongly electron-withdrawing group used for the recognition of thiol or selenol. Moreover, 2,4-dinitrophenyl ether and 2,4-dinitrobenzenesulfonamide have superior abilities to distinguish between selenol and thiol than the 2,4-dinitrobenzenesulfonate group. Sel-green has been used to quantify the content of Sec in TxR and to detect Sec in HepG2 cells. When Sel-green was used to stain cells to study the cytotoxicity of selenium compounds, it was found that highly toxic compounds also showed a positive signal, indicating that their toxicity depends on their ability to metabolize into selenol in cells. The response time of the probe to Sec was 3 min, the detection range of selenium compounds under physiological conditions was 0–100 μM, and the detection limit was 62 nM. Sel-green was the first probe capable of selectively recognizing Sec under physiological conditions.

Wang et al. combined an NBD fluorophore with a 2,4-dinitrobenzenesulfonyl group via a secondary amine group to synthesize a probe (Fig. 1, panel **8**) for specifically detecting PhSH [142]. Since the pK_a of PhSH is about 6.5, whereas that of an aliphatic thiol is about 8.5, in a physiological environment, the dissociation of high levels of PhSH will generate the corresponding thiolate, which can effectively react with benzenesulfonamide. Aliphatic thiols are maintained in a neutral form with lower reactivity, such that sulfonamide cleavage is very slow. The probe showed λ_{ex} = 465 nm and λ_{em} = 555 nm, and the detection limit for PhSH was 0.2×10^{-5} M.

Yang et al. have long studied the pK_a transformation mechanism of the Schiff-base structure of hemicyanine, and developed a long-wavelength fluorescent probe (MC-Sec) for the detection of selenol by introducing a strongly electron-withdrawing 2,4-dinitrobenzenesulfonyl group (Fig. 1, panel **9**) [143]. The pK_a value of MC-Sec is 6.40. At physiological pH, it mainly exists in the form of its Schiff base and shows no fluorescence. When Sec is added to its solution, Sec and the probe MC-Sec undergo a nucleophilic substitution reaction, releasing the fluorophore with a higher pK_a value (pK_a = 9.0). Therefore, under physiological conditions, the fluorophore mainly exists in the form of a protonated Schiff base, which causes the absorption wavelength of the detection system to be red-shifted and the fluorescence intensity to increase significantly. The probe showed high selectivity and sensitivity for the detection of selenol, λ_{ex} = 550 nm, λ_{em} = 593 nm, the detection range was 0–70 μM, and the limit of detection was 68 nM. The probe could be applied in serum and live cells.

Chen et al. synthesized a fluorescent probe, Mito-di NO_2 (Fig. 1, panel **10**), for detecting selenol, by connecting a 2,4-dinitrobenzenesulfonamide responsive group with a lipophilic triphenylphosphine cationic mitochondrial targeting group to a near-infrared (NIR) heptamethine cyanine fluorophore [144]. The probe showed a rapid response to selenol within 4 min. Since the introduction of a methyl group makes the amide bond form a tertiary amine, a certain degree of steric hindrance can be generated, but it is not affected by some macromolecular RSeS during detection. At the same time, it is more difficult to cleave than the above sulfonamide bond, so it should be free from the interference of RSS, ROS, RNS, metal cations, and anions. This probe could be used to target mitochondria and quantify the selenol concentrations in BRL 3A, RH-35, HL-7702, HepG2, and SMMC-7721 cell lines. It has been successfully used to detect changes in the concentration of selenium in a model of mitochondrial-related acute cell inflammation induced by CS_2, and to evaluate the protective effect of selenium on acute/chronic hepatitis induced by CS_2.

Carbon dots (CDs) have received much attention due to their unique optical properties, high photostability, biocompatibility, and low toxicity [145]. Li et al. used *m*-aminophenol as a carbon source to synthesize and screen CDs with yellow-green fluorescence, and covalently coupled 2,4-dinitrobenzenesulfonyl to the surface of carbon quantum dots through a sulfonamide bond. A CD-based fluorescent probe for specifically detecting Sec was thereby obtained (Fig. 4, panel **11**) [146]. The probe showed excellent sensitivity and specificity for Sec. Preliminary studies showed CD-DNS to be of low toxicity, to have optical parameters of λ_{ex} = 450 nm and λ_{em} = 514 nm at pH 4.94–9.18, and to show excellent sensitivity and specificity for Sec with a limit of detection of 23 nM. This makes them suitable for fluorescence imaging of exogenous and endogenous selenol in living cells.

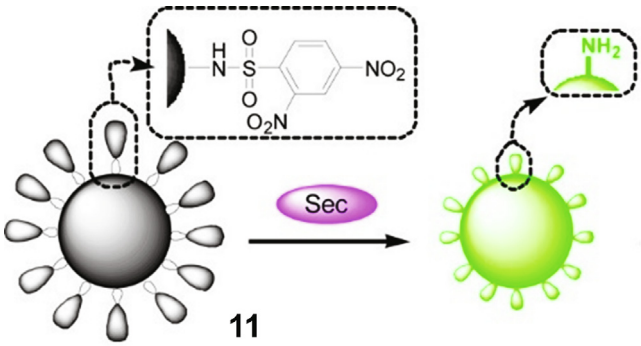

Fig. 4. Strategy for detection of Sec by probe 11 [146].

2.2. Phenyl ethers as the detection groups

The use of phenyl ethers as the detection group is the main research direction of fluorescent probes based on S_NAr reactions for RSS and RSeS [147–152]. Cleavage of the carbon-chalcogen bonds in phenyl-O ethers, phenyl-S ethers, and phenyl-Se ethers becomes increasingly facile as the atomic radius increases on going from oxygen to sulfur to selenium. In addition, the introduction of appropriate groups at different positions on the benzene ring can also modulate the ease of dissociation of phenyl ethers [153–155].

2.2.1. Phenyl-O ether as the detection group

With phenyl-O ether as the reaction site of the probe, selenol or thiol will break the phenyl-O ether bond, and thereby become bound to the aromatic moiety of the detection group. The probe is displaced by the quenching group, and the enhanced fluorescence provides the detection signal [156–160]. Response times of phenyl-O ether groups to the detection group of RSS and RSeS are longer, the selectivity is not high, but the fluorescence is strong [161]. However, introducing electron-withdrawing groups at other positions on the benzene ring of the detection group can shorten response times and quench the fluorescence of the fluorophore [162–166]. Therefore, for RSS and RSeS with low pK_a values, nitrophenyl-O ethers are good choices [167–170].

Feng et al. have studied the benzopyranonitrile moiety. A fluorescent probe (Fig. 5, panel **12**) for detecting Sec was synthesized by introducing 2,4-dinitrophenyl ether into a benzopyranonitrile fluorophore [171]. This probe was used to detect Sec in bovine serum samples and exogenous and endogenous Sec in live cells. The probe (λ_{ex} = 560 nm, λ_{em} = 706 nm) showed good linearity in the Sec concentration range 0.2–80 mM, with a detection limit of 62 nM. Although the detection limit of this probe is slightly higher, the larger Stokes displacement is more conducive to naked eye observation.

Graphene quantum dots (GQDs) are endowed with excellent solubility, biocompatibility, highly adjustable photoluminescence (PL), excellent light stability, good cell permeability, easy functionalization, and low cost. They are widely used in the field of fluorescent probes. The photoluminescence properties of GQDs are highly sensitive to light-induced electron-transfer phenomena due to their extremely small size and related quantum confinement

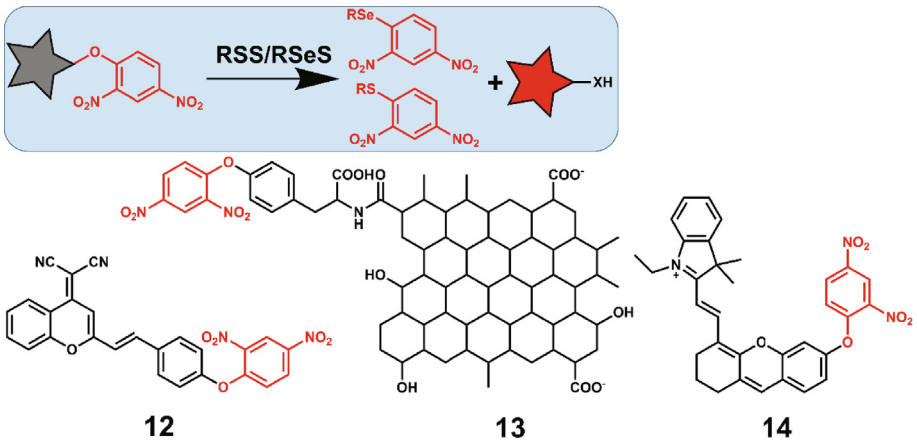

Fig. 5. Phenyl-O ether-based RSS/RSeS-specific fluorescent probes and their detection mechanisms.

effects. Chen et al., based on the formation of phenyl-O ethers with 2,4-dinitrophenyl and tyrosine to functionalize GQDs, developed H_2S-specific fluorescent probes (Fig. 5, panel **13**) and used them to respond to the real-time dynamic changes of intracellular H_2S levels in response to stimulation imaging [172]. At physiological pH, the detection limit was as low as 0.05 nM, and the maximum linear response was as high as 30 nM, with optical parameters of λ_{ex} = 480 nm and λ_{em} = 534 nm.

Wu et al. have long studied thiol probes, introduced 2,4-dinitrophenyl-O ether groups into external cyanine NIR dyes, and synthesized H_2S-specific dual-mode fluorescent probes (Fig. 5, panel **14**). These could be used to image endogenous H_2S in tumor-bearing HCT-116 mice [173]. More importantly, they could also be used to monitor metformin-induced liver injury in mice by detecting liver H_2S. With the help of multispectral optoacoustic tomography (MSOT), the probe could be successfully used to distinguish, accurately locate, and assess the volume of liver damage. In addition, the probe NR-NO_2 showed quite good response specificity, sensitivity to H_2S, and good biosecurity; with optical parameters of λ_{ex} = 680 nm and λ_{em} = 725 nm, its limit of detection was 40 nM.

Based on an assembly of tetrastyrene, 3-hydroxyflavone, and 2,4-dinitrophenyl-O ether, Wu et al. also designed and synthesized an H_2S-specific fluorescent probe with aggregation-induced emission (AIE) and excited-state intramolecular proton transfer (ESIPT). A cationic liposome was used to encapsulate the probe TPE-1, endowing it with enhanced biocompatibility, water solubility, and cell uptake capacity (Fig. 6, panel **15**) [174]. The probe had a diameter of 72.31 nm, a polydispersity index (PDI) of 0.218, a zeta potential of 56.9 mV, optical parameters of λ_{ex} = 452 nm and λ_{em} = 550 nm, and a low detection limit of 55 nM. At physiological pH, the cationic liposome nanoprobe showed good stability and detection capability, reaching equilibrium within about 5 min. The detection mechanism shows that cleavage of the phenyl ether bond occurs due to the nucleophilic nature of H_2S, the hydroxyl group is deprotected, intramolecular proton transfer is restored, and an intramolecular hydrogen bond is formed. As a result, internal rotation of the tetrastyrene structure is restricted, and the aggregate is fluorescent. The probe permitted fluorescence imaging of endogenous H_2S in cells and of exogenous H_2S in zebrafish.

2.2.2. Phenyl-S ether as the detection group

For probes that use phenyl-S ether as the reaction site, since sulfur already occupies the binding site on the detection group, when the analyte breaks the phenyl-S ether bond, both the analyte

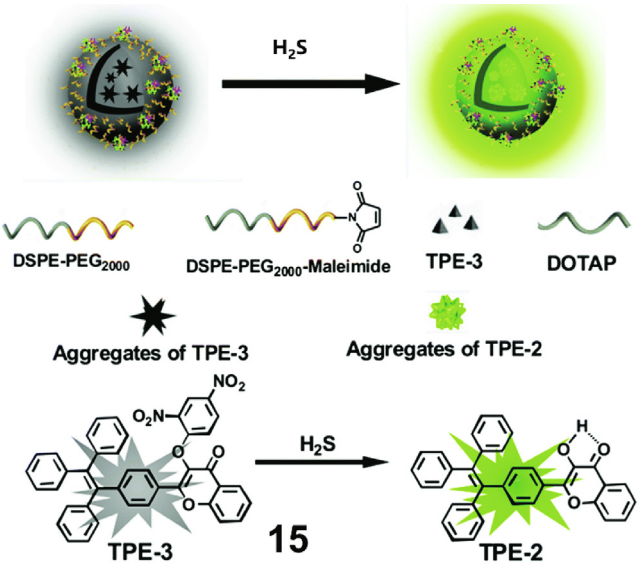

Fig. 6. Strategy for detection of H_2S by probe 15 [174].

and the fluorophore are covalently bonded with sulfur; due to the concomitant loss of the quenching group, the fluorescence of the probe is changed, providing the detection signal [175–177]. The appending of electron-withdrawing groups on the benzene ring of the detection group can shorten response times. Compared with the phenyl-O ether group, the phenyl-S ether group responds to RSS more quickly [100,154]. At the same time, because the analyte forms a covalent bond with the fluorophore rather than the detection group, the steric effect and covalent bond can be combined to distinguish glutathione from Cys/Hcy [100,101]. However, when the phenyl-S bond is strong, it is not only not less likely to react with RSS, but also less likely to be oxidized by ROS. Fortunately, because the valence state of S increases after oxidation, it is easily reduced by S with a lower valence state, so it readily reacts with RSS with lower pK_a values [178,179].

Zhang et al. have studied BODIPY fluorescent probes for a long time. By introducing a phenyl-S ether group at the 8-position of BODIPY, they developed a selective fluorescent probe for detecting GSH (Fig. 7, panel **16**) [180]. The detection of two emission channels allowed the distinction of GSH from Cys and Hcy, with only the latter two inducing intramolecular ammonolysis of thioether. The probe could be used to detect GSH within 30 min, with λ_{ex} = 480 nm and λ_{em} = 535 nm, and the detection limit was 10 nM. Concomitantly, the detection of Cys and Hcy could also be achieved within 6 min, with λ_{ex} = 390 nm and λ_{em} = 462 nm. Colorimetric or fluorescence observation can be conveniently applied to measure the content of GSH in human plasma.

Chen et al. designed a fluorescent probe for detecting GSH based on a cyanine dye as the fluorophore and 3,5-bis(trifluoromethyl)thiophenol as the detection group (Fig. 7, panel **17**) [181]. The detection limit of the probe for GSH was 3.3 × 10^{-7} M, with λ_{ex} = 780 nm and λ_{em} = 805 nm. After reacting with Cys or Hcy, the emission wavelength of the probe was blue-shifted, and the fluorescence intensity was weakened (λ_{em} = 740 nm, λ_{ex} = 650 nm). The probe was also used for imaging GSH in living cells and for fluorescence detection of GSH in SCC7 tumor-bearing mice.

Yang et al. introduced a triethylene glycol group at the 3-position of the BODIPY framework through a click reaction to improve its water solubility. At the 5-position, *p*-nitrothiophenol or *p*-nitrophenol was introduced to synthesize fluorescent probes for Cys (Fig. 7, panels **18a** and **18b**) [151]. The amino group of Cys can undergo rapid intramolecular substitution through a five-membered-ring transition state to generate amino BODIPY, causing blue shifts in the absorption and emission spectra. The six-membered-ring transition state of Hcy is similar, but the reaction rate is slower, and it exists in the form of thiol-BODIPY, reacting with GSH in a certain time. The significant difference in the photophysical forms of BODIPY substituted by amino and mercapto can be used to distinguish Cys from Hcy/GSH. Because the phenyl-S ether bond is less stable than the 2,4-dinitrophenyl ether bond, *p*-nitrothiophenol is more easily cleaved than *p*-nitrophenol. Consequently, probe **18a** shows faster reaction rates than probe **18b**, and the former is more suitable for detecting thiols. The detection range of **18a** is 0–100 μM, with λ_{ex} = 528 nm and λ_{em} = 588 nm, and the detection limit is as low as 2.12 × 10^{-7} M.

Zhao et al. used 1,3,5,7-tetraaryl-substituted BODIPY compounds with large steric hindrance and long absorption wavelength as fluorophores and 4-methoxyphenyl-S ether as a detection group to assemble two fluorescent probes (Fig. 7, panels **19a** and **19b**) for the detection of Cys and Hcy [182]. The detection of Cys and Hcy by probe **19a** was complete within 30 min, with λ_{ex} = 470 nm and λ_{em} = 581 nm. The detection range was 0–15 μM, and the limits of detection were 44 nM for Cys and 63 nM for Hcy. The detection of Cys by probe **19b** was complete within 90 min, with λ_{ex} = 525 nm and λ_{em} = 608 nm. The detection range for Cys was 0–25 μM, and the limit of detection was 286 nM. The slower rate for **19b** was attributed to the increased steric congestion of the 1,7-diphenyl moieties in the conformationally restricted BODIPY dye. Both of these fluorescent probes were successfully applied for the selective imaging of Cys and Hcy in living cells.

Yin et al. combined the heptocyanine fluorophore with *p*-aminothiophenol through a thioether bond to synthesize a fluorescent probe (Fig. 7, panel **20**) for detecting GSH [183]. The probe (λ_{ex} = 710 nm, λ_{em} = 818 nm) showed a detection range of 0–30 μM its reaction reached equilibrium within 40 min, and the limit of detection was 20 nM. The probe showed good water solubility, biocompatibility, and cell permeability, coupled with low cytotoxicity, making it an effective biomarker for monitoring GSH levels in living cells.

In 2008, Burgess et al. reported a series of amine- and thiol-regulated pyrrole dyes [184]. Interestingly, their aminopyridine red dye had λ_{ex} = 460 nm and λ_{em} = 540 nm, whereas their mercap-

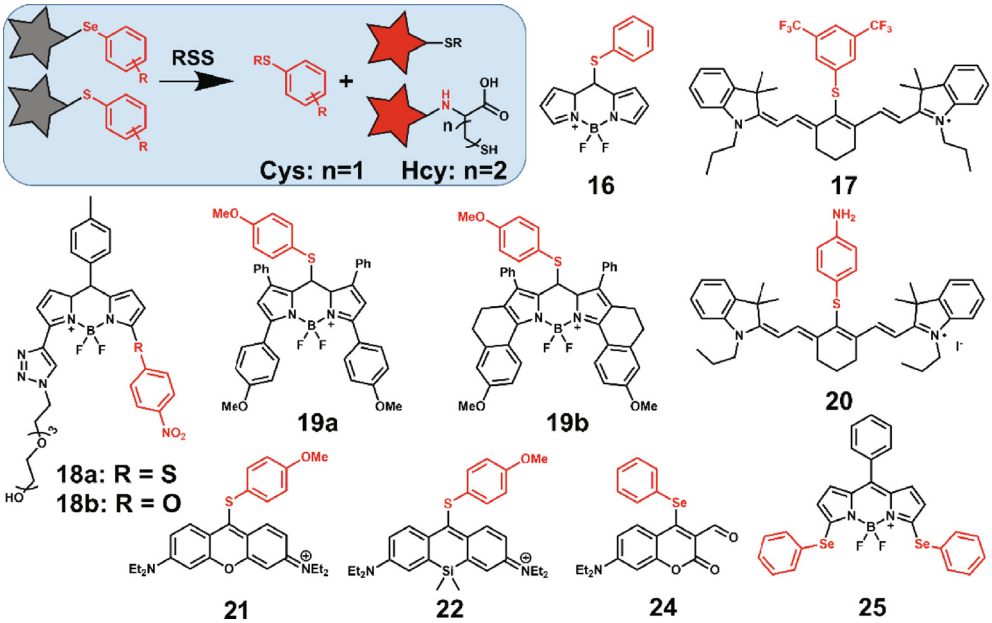

Fig. 7. Phenyl-S ether and phenyl-Se ether-based RSS-specific fluorescent probes and their detection mechanisms.

topyridine red dye had significantly red-shifted absorption and emission wavelengths (λ_{ex} = 598 nm, λ_{em} = 619 nm). Inspired by this report, Guo et al. connected 4-methoxythiophenol with pyrochrome to design a probe (Fig. 7, panel **21**) for detecting thiols [185]. This probe could be deployed in phosphate-buffered saline (PBS), and the simultaneous monitoring of two near-infrared (NIR) channels allowed the selective detection of Cys/Hcy and GSH. This was accompanied by fast reaction kinetics and an obvious fluorescence turn-on response. The reaction time of this probe with Cys (Hcy) was 15 min, with λ_{ex} = 455 nm and λ_{em} = 546 nm, and the detection range was 0–60 μM. The reaction time with GSH was 2 min, with λ_{ex} = 580 nm and λ_{em} = 622 nm, and the detection range was 0–1.0 mM. Because intracellular concentrations of Cys and GSH are in the ranges 30–200 μM and 1–10 mM, respectively, the probe is sufficiently sensitive to image biothiols in cells [186,187].

In a follow-up study, Guo et al. introduced Si into the rhodamine fluorophore and designed a cysteine-specific fluorescent probe with 4-methoxythiophenol as the detection group (Fig. 7, panel **22**) [188]. The detection range of this probe for Cys was 0–2 μM, with λ_{ex} = 488 nm and λ_{em} = 620 nm, and the limit of detection was 2.6 nM. The probe initially reacted non-selectively with Cys and GSH to form a fluorescent Cys adduct and a non-fluorescent GSH adduct. However, the GSH in the latter could be further replaced by Cys to produce more of the former, overcoming the problem of probe consumption by GSH. Therefore, the presence of GSH is not problematic for the specific detection of Cys. Importantly, the deployment of this probe not only proved that inhibiting cysteine/glutamate antiporter (system xc^-) is more effective in sensitizing cancer cells to chemotherapy than inhibiting glutamate-cysteine ligase (GCL), but also revealed a possible self-protection mechanism of cancer cells. When extracellular Cys is blocked, cancer cells can still survive by exporting intracellular GSH/GSSG as a source of Cys to provide intracellular Cys to resist harmful oxidative stress. The probe also confirmed that disrupting self-protection is a more effective strategy for sensitizing cancer cells to chemotherapy.

A near-infrared zone two (NIR-II) fluorescent probe can realize high-resolution biological imaging with deep tissue penetration. However, due to a lack of target specificity, existing NIR-II materials usually have a poor signal-to-noise ratio. Zhao et al. encapsulated an H_2S-responsive fluorescent probe in a hydrophobic core–shell silica nanocomposite so as to assemble an activatable NIR-II nanoprobe to visualize colorectal cancer cells (Fig. 8, panel **23**) [189]. The detection range of this nanoprobe for H_2S was 0–10 μM, and the limit of detection was 37 nM, with λ_{ex} = 520 nm and λ_{em} = 780 nm. Although the maximum emission wavelength was 900 nm, the emission spectrum was quite broad and extended to the NIR region II (1000–1300 nm). The probe reaction reached equilibrium within 5 min, and could be used to monitor H_2S and related biological processes in real time. This nanoprobe showed a specific and proportional fluorescence response to H_2S, and could be used to selectively identify H_2S-rich colon cancer cells and to distinguish live cell types based on their differences in H_2S contents in a two-color imaging mode. More importantly, H_2S specifically activates fluorescence in the NIR-II region, and the probe can detect and distinguish cancer in vivo by taking full advantage of the depth and spatial resolution of NIR-II imaging.

2.2.3. Phenyl-Se ether as the detection group

For probes that use phenyl-Se ether as the reaction site, when the analyte breaks the phenyl-Se ether bond, since selenium already occupies the binding site on the detection group, the analyte is forced to form a covalent bond with the fluorophore [103,104]. At the same time, the fluorescence of the probe is enhanced due to the loss of the quenching group, and this provides the detection signal. The response of the phenyl-Se ether group to RSS is faster than those of phenyl-O ether and phenyl-S ether. Because the analyte forms a covalent bond with the fluorophore instead of the detection group, steric hindrance and different combination modes may be exploited to distinguish GSH, Cys/Hcy, H_2S, and so on. Phenyl-Se ether can also be oxidized by ROS, and the latter may be detected on the basis of the resulting fluorescence changes. Conversely, RSS will reduce selenium and restore fluorescence [190,191].

Churchill et al. inserted a phenyl-Se ether moiety at the 4-position of coumarin to synthesize a fluorescent probe capable of specifically detecting GSH (Fig. 7, panel **24**) [103]. This functional group can quench the fluorescence of coumarin by PET and can also act as a leaving group. The aldehyde group at the 3-position also plays a dual role: it enhances the electrophilicity of the Michael acceptor at the 4-position, while also inducing the cyclization reaction of the thiol and primary amine groups of Cys/Hcy. When the probe reacts with GSH, the latter is inserted at the 4-position of coumarin in the form of a thioether. Due to steric hindrance, the amino group of GSH can only attack the 3-position with respect to the aldehyde group, causing GSH and the fluorophore to form a ring structure, increasing the conjugation of the system. Concomitantly, the amino group forms an internal hydrogen bond with the adjacent carbonyl group, and the fluorescence is enhanced. The limit of detection of the probe for GSH was 2.7×10^{-7} M, with λ_{ex} = 471 nm and λ_{em} = 518 nm, the detection range was 0–40 μM, and equilibrium was attained within 100 ms (as determined by UV/Vis monitoring). Cys/Hcy will form a secondary amine group at the 4-position of coumarin. Cys/Hcy also undergo a cyclization reaction with the aldehyde group in the 3-

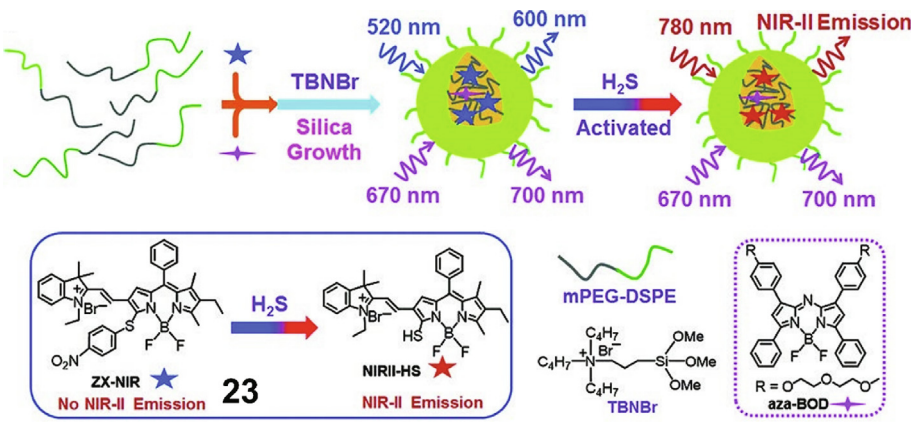

Fig. 8. Strategy for detection of H_2S by probe 23 [189].

position, decreasing the fluorescence. The probe has also been successfully used for imaging GSH in Hep3B cells.

Qin et al. introduced phenyl-Se ether groups at the 3- and 5-positions of the BODIPY framework to synthesize fluorescent probes (Fig. 7, panel **25**) for detecting H_2S [104]. In the presence of excess H_2S, the second phenyl-Se ether group of the probe was substituted, and the fluorescence emission intensity was further reduced. The detection range of this probe for H_2S was 0–15 μM, the limit of detection was as low as 2.5 nM, and the detection reached equilibrium within 20 min, with λ_{ex} = 582 nm and λ_{em} = 610 nm. The fluorescence of the probe is shut down by H_2S, providing excellent sensitivity and selectivity for its detection. It has been widely used in intracellular H_2S detection and fluorescence microscopy imaging.

2.3. NBD as the detection group

Probes that use NBD as a reactive group can be mainly classified into those with an NBD-O ether, an NBD-S ether, or an NBD-N bond [111,192–196]. When forming the above structures, NBD will show different fluorescence emissions, making it suitable to distinguish different RSSs [197–204].

2.3.1. NBD-O ether as the detection group

With NBD-O ether as the detection group of a probe, after the RSS breaks the NBD-O ether bond, the fluorescence of the fluorophore recovers, and the analyte concomitantly forms a covalent bond with the NBD to achieve the purpose of detection [205–207]. Since an NBD-S bond will quench the fluorescence of NBD, H_2S, PhSH, GSH, and thiol-containing proteins cannot restore it. Therefore, NBD-O ether can be used for distinguishing Cys or Hcy from other RSSs based on the fluorescence recovery of fluorophores and the change of NBD fluorescence [208–211].

Ma et al. combined NBD with the hydroxyl group of resorufin to synthesize a specific fluorescent probe for distinguishing GSH from Cys/Hcy, which showed unique emission modes of Cys and GSH at only one excitation wavelength (Fig. 9, panel **26**) [212]. Upon reaction with Cys/Hcy, this probe releases the amino NBD and resorufin (λ_{ex} = 470 nm, λ_{em1} = 540 nm, λ_{em2} = 585 nm), but only one emission is seen after reaction with GSH (λ_{em} = 585-nm). Evidently, the sulfur atom of GSH quenches the fluorescence of NBD, but due to steric hindrance the amino NBD cannot be formed. The limits of detection of Cys and GSH at λ_{em} = 585 nm were determined as 0.13 μM and 0.07 μM, and the detection ranges were 1–40 μM and 1–18 μM, respectively. The probe was also applied for the detection of Cys and GSH in human plasma samples, with recovery rates of 95–109% and 102–104%, respectively.

Feng et al. introduced NBD-O ether, methyl, and aldehyde groups at the 2-, 3-, and 5-positions, respectively, of a 2-(2-hydroxyphenyl)benzothiazole (BHT) fluorophore, and thereby synthesized a highly selective fluorescent probe for the detection of H_2S (Fig. 9, panel **27**) [213]. The detection range of this probe for H_2S was 0–50 μM, the limit of detection was 150 nM, with λ_{ex} = 382 nm and λ_{em} = 455 nm, and the detection reaction reached equilibrium within 500 s. Since a methyl group is present at the *ortho* position of the NBD-O ether, there is a certain degree of steric hindrance, which greatly slows the rates of the thiolysis reactions of Cys, Hcy, and GSH. Therefore, probe **27** can also recognize H_2S with high selectivity and high sensitivity. Indeed, this probe has been used for intracellular H_2S detection and fluorescence microscopy imaging.

Lin et al. synthesized a fluorescent probe for the specific detection of thiols through combining the hydroxyphenyl benzothiazole merocyanine (HBTMC) fluorophore and the NBD fluorophore (Fig. 9, panel **28**) [214]. Cys/Hcy cleave the NBD-O ether, release the HBTMC unit (λ_{ex} = 550 nm, λ_{em} = 609 nm), and form amino NBD (NBD-Cys/Hcy, λ_{ex} = 470 nm, λ_{em} = 546 nm) through a sequence of nucleophilic substitution and intramolecular rearrangement, lighting up in green and red. GSH can generate free HBTMC1 and dark-colored thio-NBD (NBD-GSH) through a one-step nucleophilic substitution reaction, eliciting only red emission. H_2S is a stronger nucleophile, and the ether bond will also be cleaved, resulting in dark thiol-NBD (NBD-SH) and free HBTMC (HBTMC1). HS^- will further undergo an addition reaction with the double bond of HBTMC1 to form an HBTMC derivative (HBTMC-SH, λ_{ex} = 410 nm, λ_{em} = 485 nm), resulting in a new blue emission. On further adding H_2S to a mixture of probe **28** and Cys/Hcy or probe **28** and GSH, the intermediate products NBD-Cys/Hcy or NBD-GSH will be further substituted, and HBTMC1 will be attacked by HS^- anions to produce dark NBD-SH and blue fluorescent HBTMC-SH, accompanied by quenching of the green and red

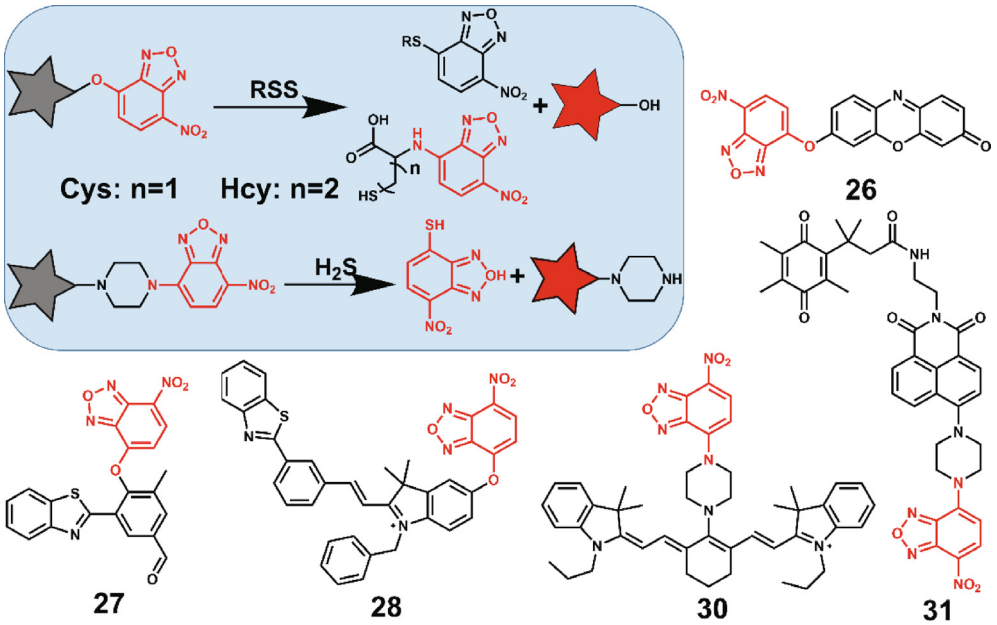

Fig. 9. NBD-based RSS-specific fluorescent probes and their detection mechanisms.

emission. In summary, probe **28** can distinguish Cys/Hcy, GSH, and H_2S by the change order of three clearly defined emission bands (blue, green, and red). The limits of detection of this probe for Cys, Hcy, GSH, and H_2S were 4.25, 5.11, 4.30, and 6.74 μM, respectively. The unique design of probe **28** may open the way to the design of other fluorescent probes for distinguishing and sequentially detecting biothiols, providing hope for revealing the interrelated effects of biothiols under various physiological and pathological conditions.

2.3.2. NBD-S ether as the detection group

In contrast to the previous case, for probes with NBD-S ether as the reaction site, after the NBD-S ether is cleaved by RSS, the fluorescence of the NBD group is quenched by sulfur, and the analyte and fluorophore are forced to form a covalent bond. The quenching effect of sulfur depends on its distance from the fluorophore; if the distance is larger than 0.6 nm, the quenching effect will be weak or non-existent. The quenching ability of sulfur is only moderate, much weaker than that of a nitro group. Only Cys/Hcy can form a covalent bond with the fluorophore through the amino group to restore the fluorescence [107,110,111].

Shao et al. appended NBD fluorophores on the surface of gold nanoclusters to assemble a ratiometric fluorescent probe for the detection of Cys and Hcy (Fig. 10, panel **29**) [215]. The probe reacted with Cys and Hcy to form amino NBD and gold nanoclusters, with λ_{ex} = 410 nm, λ_{em1} = 485 nm, and λ_{em2} = 540 nm. The detection ranges for Cys and Hcy were 8.33–100 μM and 16.67–100 μM, with limits of detection of 1.45 μM and 1.8 μM, respectively. The probe was also successfully used for fluorescence imaging of Cys and Hcy in HeLa cells, giving good results.

2.3.3. NBD-N as the detection group

For probes with NBD-N as the reaction site, after an RSS breaks the NBD-N bond, the fluorescence of the NBD group is quenched by S, and the fluorescence of the fluorophore is enhanced due to exposure of the amino group, which provides the detection signal [216–218].

Yi et al. have long studied NBD fluorophores and thiol probes. They connected an NBD fluorophore to a cyanine dye through a piperazine moiety to synthesize an NIR fluorescent probe capable of selectively detecting H_2S in vivo (Fig. 9, panel **30**) [219]. The detection range of this probe for H_2S was 0–100 μM, and the limit of detection was 39.6 nM, with λ_{ex} = 730 nm and λ_{em} = 796 nm (87-fold fluorescence enhancement). Biological imaging results showed that: (1) D-Cys can induce the production of endogenous H_2S in living cells and stimulate angiogenesis; (2) intravenous injection of the probe into the tail of a mouse produces strong fluorescence in its liver, and intraperitoneal injection of D-Cys can further enhance the fluorescence from the liver; (3) intratumoral injection of the probes allows the rapid and selective detection of endogenous H_2S in colorectal cancer cells (HCT116, HT29) in vitro and in mouse tumor models. These results indicate that the probe can be used as an effective tool for detecting H_2S and even cancer in living animal cells.

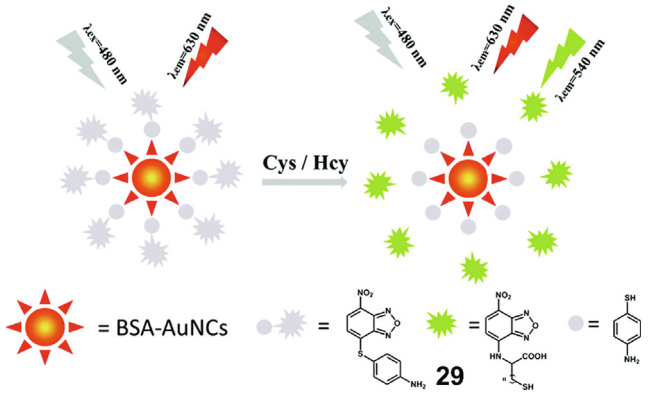

Fig. 10. Strategy for detection of Cys/Hcy by probe 29 [215].

Yi et al. used trimethyl-lock containing quinone propionic acid (Q_3PA) as the detection group for human NADPH: quinine oxidoreductase 1 (hNQO1), NBD-N as a detection group for H_2S, and naphthalimide as a fluorophore. These were assembled to form a fluorescent probe showing dual responses to H_2S and hNQO1 (Fig. 9, panel **31**) [220]. The probe only showed enhanced fluorescence in the simultaneous presence of H_2S and hNQO1; the single components alone did not elicit a response. It showed high sensitivity, excellent selectivity, and good biocompatibility, with λ_{ex} = 465 nm and λ_{em} = 535 nm. This allowed us to distinguish the activation levels in HT29 and HepG2 cells from those in FHC, HCT116, and HeLa cells, due to the significantly different endogenous levels of H_2S and hNQO1 in these cell lines.

2.4. Benzoate as the detection group

Common benzoate detection groups include 4-nitrobenzoate, 2-fluoro-5-nitrobenzoate, 2-selenobenzoate and thiobenzoate. When benzoate or thiobenzoate is used as the reaction site, the analyte breaks the original ester bond and generates a new thiobenzoate. At the same time, the probe is quenched by the quenching group. The associated fluorescence changes provide the detection signal [221–228].

2.4.1. Benzoate-O as the detection group

Chen et al. used heptamethine cyanine dye as the fluorophore and 4-nitrobenzoate as the detection group (Cy-NB) to synthesize an NIR ratiometric fluorescent probe (Fig. 11, panel **32**) for detecting Cys [229]. Its optical parameters were λ_{ex} = 720 nm and λ_{em} = 785 nm. Cys forms a thiobenzoate with the 4-nitrobenzoic acid group. The π-electron system of the fluorophore is modified upon conversion from the enol form to the ketone form, and a spectral shift occurs; λ_{ex} = 560 nm, λ_{em} = 640 nm. Using this principle, Cy-NB could be used to detect the NIR ratio of Cys through the fluorescence ratio ($F_{640\ nm}/F_{785\ nm}$). This probe could be used to detect Cys within 5 min with a detection limit of 0.2 μM, and could sensitively detect changes in Cys levels in mitochondria under different oxidative stress states in HepG2 cells. The probe was also used to detect changes in Cys levels in mice. The results indicated that mitochondrial Cys could be viewed as a biomarker for oxidative stress, offering potential for simple clinical application.

By using the characteristics of the two -SH groups in H_2S_2, Xian et al. designed and synthesized a fluorescent probe (Fig. 11, panel **33**) containing two 2-fluoro-5-nitrobenzoate groups to detect H_2S_n ($n > 1$) [230]. H_2S_2 first underwent electrophilic reaction with fluorine, and then further underwent a bimolecular aromatic nucleophilic substitution reaction (S_N2Ar) with a benzoate group to form a thioether, thereby turning on fluorescence. The fluorescence intensity of this probe was linearly related to the concentration of Na_2S_2 in the range 0.5–15 μM, and the limit of detection was approximately 71 nM, with λ_{ex} = 490 nm and λ_{em} = 515 nm. The probe was successfully used to sensitively and selectively detect H_2S_n/H_2S_2 in aqueous buffer and cells, and also served to prove that the formation of H_2S_n may be related to the reaction of H_2S and ROS (such as ClO^-).

2.4.2. Thiobenzoate as the detection group

The active site of thiobenzoate is also called a natural chemical linkage (NCL), and this reaction has been widely used in peptide synthesis [231–233]. The NCL of peptides involves reaction

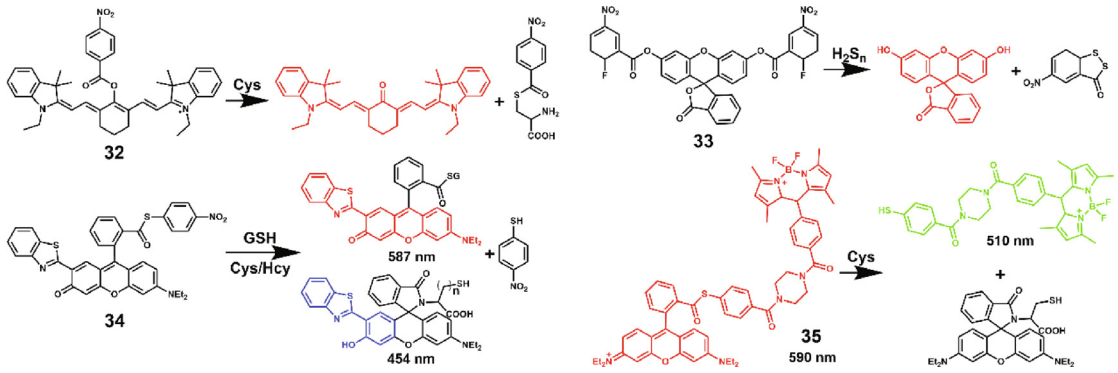

Fig. 11. Benzoate-based RSS-specific fluorescent probes and their detection mechanisms.

between a peptide α-thioester and an N-terminal cysteine peptide. The main characteristics of the NCL response include: (1) a high degree of chemical selectivity for thiols that is not disturbed by other biologically relevant species, and (2) the reaction proceeds in vivo and can be carried out in living cells. Thiobenzoate groups are a type of natural chemical linking group used to detect thiols [234].

Yang et al. combined rhodamine with *p*-nitrothiophenol to assemble a fluorescent probe that responded to GSH and Cys/Hcy (Fig. 11, panel **34**) [232]. The probe (λ_{ex} = 305 nm) reacted with Cys/Hcy to form the corresponding deconjugated spirolactam based on NCL. After adding Cys/Hcy, the fluorescence emission of the thioester intermediate (λ_{em} = 587 nm) formed by the trans-thioyl esterification reaction intensified, thus eliminating the 4-nitrobenzene-induced PET quenching process. Over time, the intramolecular S,N-acyl group shifted to form the corresponding amide (λ_{em} = 454 nm). This amide was further spirocyclized to obtain a colorless lactam under neutral conditions. The process was completed within minutes. In the presence of GSH, only the thiobenzoate group transfer reaction proceeded, thereby eliminating the PET process caused by the electron-deficient 4-nitrobenzene moiety and thus the emission band of rhodamine (λ_{em} = 587 nm). A large fluorescence enhancement was observed, and the fluorescence intensity reached a stable level within 10 min. The detection ranges of this probe were 1–10 mM for GSH and 30–200 μM for Cys, and the limits of detection for Cys, Hcy, and GSH were determined as 44, 52, and 96 nM, respectively. The probe was also successfully applied to the detection of GSH and Cys in serum and cells.

Lin et al. designed a ratiometric fluorescent probe for the detection of thiols based on NCL (Fig. 11, panel **35**) [235]. The probe consisted of a rhodamine dye, a thiobenzoic acid ester group, and a BODIPY dye. According to the NCL reaction, Cys attacks the electrophilic carbon of the thioester group to form a new thiobenzoate, which leads to cleavage of the dimer showing fluorescence resonance energy transfer (FRET). Upon reaction of the probe (λ_{ex} = 470 nm) with Cys, the BODIPY group (λ_{em} = 510 nm) is released, the emission intensity of the rhodamine group (λ_{em} = 590-nm) decreases, and FRET is turned off. The detection range of the probe for Cys was 0.1–100 μM, the detection limit was 82 nM, and reaction equilibrium was reached in 30 min. The probe was also used for FRET-based ratiometric imaging of thiols in living cells.

2.5. Phenylselenamide as the detection group

Ebselen (2-phenyl-1,2-benzisoselenazol-3(2*H*)-one) is well known as a glutathione peroxidase (GPx) mimic [236–238]. The catalysis of GPx activity by this drug may be related to the cleavage of Se-N bonds by thiols. A thiol can form selenium sulfide with the detection group; therefore, phenylselenamide can be used as the active site of a probe for RSS [239,240]. Since GPx is a selenium enzyme, such a group can be expected to be useful for RSeS detection.

Tang et al. inserted *m*-trifluoromethylbenzylphenol into the amine group of rhodamine to synthesize a fluorescent probe for detecting thiols (Fig. 12, panel **36**) [241]. When the probe reacts with a thiol, it forms a selenium-sulfur bond with the detection group, resulting in exposure of the amino group fluorophore, and the fluorescence is turned on to realize detection of the thiol. This probe (λ_{ex} = 525 nm, λ_{em} = 550 nm) showed a good linear relationship with the concentration of GSH, the detection range was 3.0–120 nM, and the limit of detection was 1.4 nM. This probe was successfully applied to thiol imaging in HL-7702 and HepG2 cells with high sensitivity and selectivity.

Chen et al. inserted 2-nitrophenylselanyl and 3-(trifluorome thyl)phenylselanyl groups into the secondary amine group of the NIR fluorophore of heptamethrin, thereby synthesizing two fluorescent probes (Fig. 12, panels **37a** and **37b**) for the detection of thiols [242]. Probe **37a** showed a linear response to GSH concentration at 750 nm, $F_{750\ nm}$ = 16236.17 [GSH/μM] – 17657.72 (r = 0.9814), as did probe **37b**, $F_{750\ nm}$ = 6599.80 [GSH/μM] – 3179.94 (r = 0.9867). Both probes (λ_{ex} = 635 nm, λ_{em} = 750 nm) could be used to detect different levels of thiols in living cells and tissue samples.

2.6. Other fluorescent probes based on S_NAr reactions for RSS and RSeS

There have been many types of RSS- and RSeS-specific probes reliant on small aromatic molecules as detection groups. Those surveyed above are just some of the more mainstream detection groups. There are many small aromatic molecules that can bind to fluorophores and are attacked by RSS or RSeS. Below, we describe some unusual cases [243–246].

Yang et al. synthesized a fluorescent probe for the detection of thiols by connecting BODIPY and coumarin through an ether bond (Fig. 13, panel **38**) [247]. The BODIPY fluorophore was designed to react with GSH and Cys to generate distinct products with different

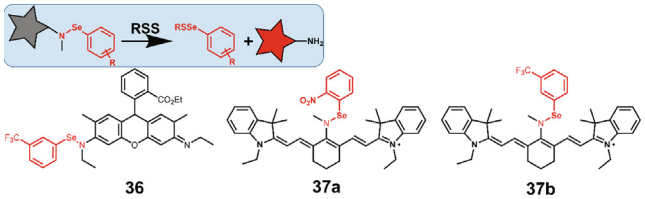

Fig. 12. Phenylselenamide-based RSS-specific fluorescent probes and their detection mechanisms.

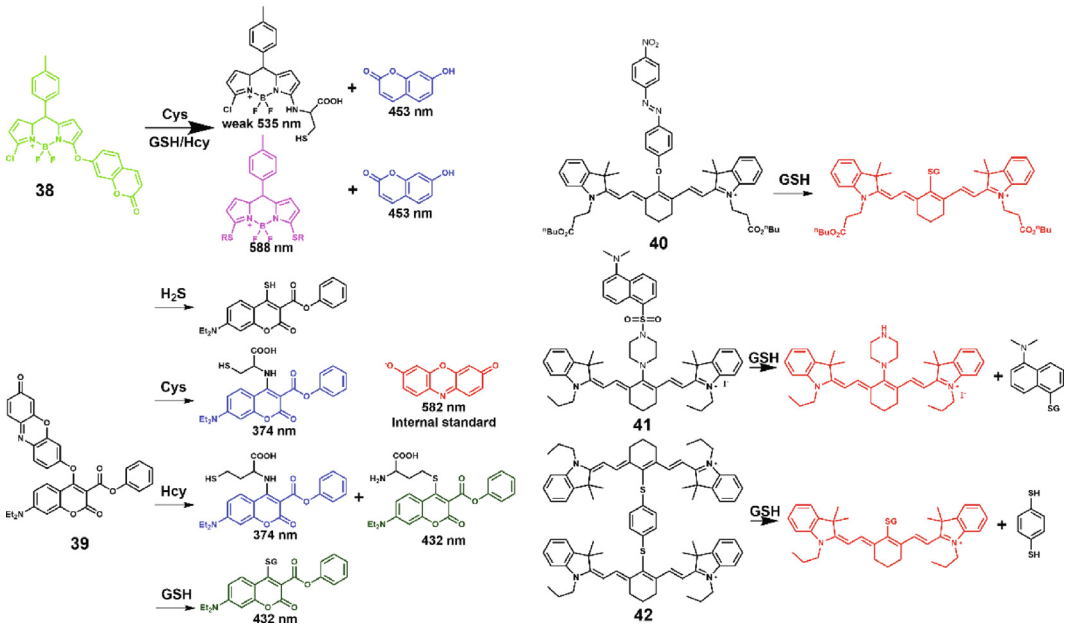

Fig. 13. Other RSS-specific fluorescent probes and their detection mechanisms.

photophysical properties, while the coumarin fluorophore served as an internal standard. This probe showed green emission in aqueous solution. After adding Cys, the N-BODIPY fluorescence produced was weak (S-BODIPY: λ_{em} = 540 nm; N-BODIPY: λ_{em} = 560 nm), and the free coumarin showed blue emission light (λ_{em} = 452 nm). In the presence of GSH, monosulfide- and disulfide-substituted BODIPY (λ_{em} = 558 nm, λ_{em} = 588 nm) and coumarin (λ_{em} = 452 nm) were generated, such that different concentrations of GSH produced various emission colors. Interestingly, the solution showed white fluorescence at a GSH concentration of 0.4 mM. The fluorescence intensity at 452 nm showed a good linear relationship with Cys concentration in the range 0–100 μM. The limit of detection was calculated as 3.66×10^{-7} M. The fluorescence intensity at 588 nm showed a good linear relationship with GSH concentration in the range 0–1 mM, with a limit of detection of 1.07×10^{-6} M. This probe was successfully used to detect Cys and GSH in living cells.

Song et al. combined 7-diethylaminocoumarin and resorufin through ether bonds to synthesize fluorescent probes for distinguishing and detecting different thiols (Fig. 13, panel **39**) [248]. These probes reacted with H_2S to release the red fluorescent resorufin (λ_{em} = 582 nm) along with non-fluorescent mercaptocoumarin, giving a strong red fluorescence signal. The probes reacted with GSH, Cys, and Hcy to not only release the red-light-emitting resorufin, but also the corresponding thiocoumarin (C-S-GSH, C-S-Cys, or C-S-Hcy; λ_{em} = 432 nm), emitting green fluorescence. Through different degrees of intramolecular rearrangement, C-S-Cys can be completely converted into a blue-fluorescent C-N-Cys (five-membered ring, λ_{em} = 374 nm), and C-S-Hcy can be partially converted into a blue-fluorescent balanced state C-N-Hcy (six-membered ring, λ_{em} = 374 nm). Because the energy of a ten-membered ring is kinetically high, C-S-GSH (λ_{em} = 432 nm) is very stable and can only maintain green fluorescence. Therefore, the probe was able to show different signal patterns for different biothiols in solution and live cells, namely red for H_2S, blue-red for Cys, blue-green-red for Hcy, and green-red for GSH.

Kim et al. used heptocyanine as the fluorophore and nitroazobenzene as the detection group to synthesize NIR fluorescent probes (Fig. 13, panel **40**) for distinguishing GSH from Cys/Hcy [249]. After adding GSH, the fluorescence spectrum of the probe showed a significant red shift of its maximum (λ_{ex} = 600 nm, λ_{em} = 810 nm), whereas the addition of Cys or Hcy elicited a weak, blue-shifted fluorescence response at λ_{em} = 747 nm. The limit of detection for GSH was 26 nM. The probe was successfully applied for cell imaging of GSH in mitochondria, showing a good response to different amounts of mitochondrial GSH in cells, and may thus be used as a mitochondrial GSH tracer.

Yoon et al. combined the heptamethine cyanine fluorophore and the dansyl detection group through a piperazine linkage to synthesize a fluorescent probe for detecting GSH (Fig. 13, panel **41**) [250]. Their probe (λ_{ex} = 730 nm, λ_{em} = 736 nm) showed high selectivity for GSH, which could be detected within 15 min. The amide group of GSH may form a hydrogen bond with the piperazine ring unit of probe **41**. There may also be electrostatic interaction between the indole cation of the probe and the carbonate anion of GSH. The interaction between these moieties may cause the thiol and sulfonamide groups to be closer together, which may be the reason for the higher reactivity of GSH. Probe **41** can be used to detect changes in the GSH concentrations in living cells due to the oxidation promoted by increased H_2O_2 concentration. In whole-body images of mice, strong fluorescence was observed in various tissues, including liver, kidney, lung, and spleen.

Chen et al. synthesized a fluorescent probe for the detection of GSH by linking two NIR fluorophores with *p*-benzenedithiol (Fig. 13, panel **42**) [181]. The limit of detection of this probe (λ_{ex} = 780 nm, λ_{em} = 805 nm) for GSH was 630 nM. When this probe was reacted with Cys and Hcy, the emission wavelength was blue-shifted (λ_{ex} = 650 nm, λ_{em} = 740 nm) and the fluorescence intensity decreased. The probe was also used to assess different concentrations of GSH in living cells and for fluorescence detection of GSH in SCC7 tumor-bearing mice.

Zhao et al. have studied thiol probes for a long time, and recently functionalized the BODIPY fluorophore with sulfoxide (Fig. 14, panel **43**) [179]. Their probe was encapsulated in core–shell silica nanoparticles to improve chemical selectivity. The inherent molecular size sieving properties of the porous silica shell prevented competing biothiols from entering the core molecular probe, while allowing specific reactions with the small target H_2S. Therefore, this strategy avoids interference from coexisting RSS and achieves highly chemically selective detection. Upon reac-

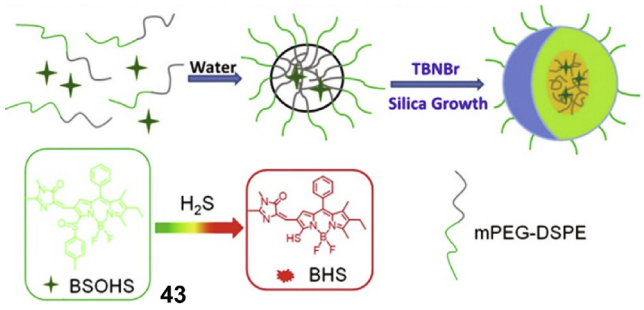

Fig. 14. Strategy for detection of Sec by probe 43 [179].

tion with H_2S, the sulfoxide group of the probe is converted into a disulfide bond, and further reacts with H_2S to displace the detection group, forming a thiol BODIPY. The absorption and emission spectra showed a clear red shift (λ_{ex} = 620 nm, λ_{em} = 713 nm). The limit of detection of the probe was 53 nM, and the detection range was 0–15 μM. The reaction rate proved to be proportional to the content of Si in the porous shell. When the particle size was 113 ± 10 nm, H_2S was equilibrated within 3 min. This probe was successfully used to detect estrogen-induced endogenous production of H_2S in cardiomyocytes and live mice.

3. Design strategy of fluorescent probes for RSS and RSeS based on S_NAr reactions

In this section, based on the integration of some reports, we propose design strategies for RSS- and RSeS-specific fluorescent probes based on S_NAr reactions. The most important aspects are the reaction sites, and the numbers and positions of substituents on the benzene ring. We also consider the influence on the S_NAr-based detection groups of some substituents or bridging groups based on other reaction mechanisms. In addition, a design strategy for RSeS-specific fluorescent probes based on S_NAr reaction is proposed. Differences in spectral properties, substituent effects, and detection targets caused by the appending different detection groups to the same fluorophore are interesting. Indeed, there have already been literature reports concerning the detection of RSS and RSeS through optimization of molecular structure. Finally, we discuss some specific design strategies that are worthy of mention.

3.1. Probe design strategies with an ether linkage as the reaction site

When constructing S_NAr-based RSS- and RSeS-specific fluorescent probes, an ether linkage is a popular choice as the reaction site [251–259]. Phenyl-O ether, phenyl-S ether, and phenyl-Se ether have mainly been used, among which the C-O, C-S, and C-Se bonds become increasingly long [161]. Although energies of these three bonds increase in sequence, S_NAr reaction becomes more likely to occur [151]. Stronger bonds are more selectively cleaved by RSS or RSeS with lower pK_a. Probe **18b** (with *p*-nitrothiophenol) is more rapidly cleaved by thiols than probe **18a** (with *p*-nitrophenol). Chen et al. constructed a probe containing a phenyl-S ether group, and its reaction with Cys reached equilibrium within 15 min [152]. Probe **25**, containing a phenyl-Se ether group, reached its initial equilibrium with H_2S within 10 min [104]. It cannot be ignored that there are large numbers of free electrons around S and Se in ether groups. These groups are thus negatively charged, making them susceptible to oxidation, especially the phenyl-Se ether group. There are already some probes for detecting ROS based on the oxidation of such linkages [178,260,261]. It is interesting that the oxidation is reversible, with reduction typically being achieved with RSS or RSeS. This also makes many RSS and RSeS probes with ether as the reaction site to be somewhat susceptible to interference from ROS in the monitoring environment. For RSS and RSeS probes with phenyl-O ether groups as the reaction site, interference from ROS in the environment is much less likely. Another benefit of using an ether as the reaction site is its quenching effect on fluorescence, which is especially notable for phenyl-S and phenyl-Se groups [104,180]. At the same time, because S or Se will leave the fluorophore as the ether group is cleaved, the test substance will be connected to the fluorophore through a covalent bond. The fluorophore will be changed through the amino group of Cys or Hcy, which constitutes a good design strategy [99–101,180].

3.2. Probe design strategies for reaction sites containing amine groups: secondary amines, tertiary amines, and piperazines

A probe containing an amine group reaction site will release this group after reacting with the analyte. Subsequent S_NAr reaction of RSS or RSeS with the detached group will cause the emission of the fluorophore to be red-shifted. Benzenesulfonamide, NBD-N, and phenylselenamide are the most commonly applied groups [142,219,241]. However, amine groups of many forms may connect the detection group to the fluorophore, such as secondary and tertiary amine groups (including piperazinyl) [131,143,144]. Compared with the benzenesulfonate group, the bond energies of the benzenesulfonamide and phenyl-O ether groups are higher, and their selectivities to RSS or RSeS are also higher [129]. Tertiary amine bonds have higher energies than oxy-ether bonds or secondary amine bonds, and have a certain steric hindrance, and their selectivity is also improved. Although a secondary amine group has a certain steric hindrance when reacting with a detection group, its pK_a is much higher than that of a tertiary amine, so S_NAr reaction is more likely to occur [144,258]. Since a conjugated system of a fluorophore decreases the pK_a of the amine group, it is also a good choice to introduce a secondary amine group (instead of a primary amine group), as this can greatly improve the yield and stability of the product. Zhang et al. appended 2,4-dinitrobenzenesulfonyl to the hydroxyl group in the 9-position of 4-amino-naphthalimide through *p*-hydroxyaniline instead of the primary amino group in the 4-position, which could be accomplished even in an extremely strongly alkaline reaction environment, and the yield of the reaction exceeded 50% [258]. Chen et al. appended 2,4-dinitrobenzenesulfonamide to the secondary amine group of the NIR heptamethine cyanine fluorophore [144], but we are not aware of any reports of appending 2,4-dinitrobenzenesulfonyl to the primary amine group of this fluorophore. Upon S_NAr reaction of RSS or RSeS probes containing a piperazine group with the analyte, two products of the detection group with piperazine and the fluorophore with piperazine may be formed at the same time [250]. The piperazine moiety can adopt a boat or chair conformation, and studies have shown that a preference for the latter conformation improves the selectivity of the probe for RSS [262–266]. Since both nitrogen atoms of piperazine can be reaction sites, the sensitivity to the analyte is increased, and the time for the reaction to reach equilibrium is greatly shortened [143,144,254].

3.3. The choice of substituents on the detection group, their position and number

Most detection groups of S_NAr-based RSS and RSeS probes contain a benzene ring framework. Hence, we consider benzene-based detection groups to discuss the choice of substituents on the benzene ring, and the effect of their position and number on selectivity. The propensity for S_NAr reaction is related to the strength and length of the bond at the reaction site.

3.3.1. Effect of different substituents on the benzene ring

The introduction of electron-withdrawing groups on the benzene ring lowers the electron density at the detection group, reduces the bond strength at the reaction site, and increases the bond length and the degree of dissociation at the reaction site [154,161]. The introduction of electron-donating groups on the benzene ring increases the electron density at the detection group, increases the bond strength at the reaction site, and decreases the bond length and the degree of dissociation at the reaction site [183]. Nitro is a typical electron-withdrawing group. The detection group of probe **18a** is *p*-nitrophenyl-S, with which detection of Cys can reach equilibrium within 200 s [151]. Without any substituents, the detection group of probe **16** is phenyl-S, with which the detection of Cys/Hcy reaches equilibrium within 6 min and the detection of GSH reaches equilibrium within 30 min [180]. Methoxy is a strongly electron-donating group. The detection group of probe **19a** is 4-methoxyphenyl-S, with which the detection of Cys/Hcy reaches equilibrium within 30 min [182]. Amino is also a strongly electron-donating group. The detection group of probe **20** is *p*-aminophenyl-S, with which the detection of GSH reaches equilibrium within 42 min [183]. Ito et al. synthesized fluorescent probes (Fig. 15) for detecting GST by connecting different detection groups to rhodamine. The four detection groups 2,4-dinitrobenzenesulfonamide, 2-nitro-4-cyanobenzenesulfonamide, 2-nitro-4-acetylbenzenesulfonamide, and 2-nitro-4-butoxy were compared [153]. The fluorescent probe with 2,4-dinitrobenzenesulfonamide as the detection group reached equilibrium of GST detection within 10 min, and the yield exceeded 80% (Fig. 15, panel **44a**). The reactions with the other three probes did not reach equilibrium in 30 min, and the yields were all below 60%. The reaction rates of the four probes were consistent with the order of the respective groups on the classic Hammett electron-withdrawing scale.

3.3.2. Effect of substituent position on the benzene ring

The position of the introduced group on the benzene ring will affect the reactivity of the active site [155,161,267]. For example, introducing a nitro group on the benzene ring will increase the degree of dissociation of the active site. From the perspective of induction effect, a nitro group attracts the electron cloud of the active site, and the closer its substitution position to the reaction site, the greater the degree of dissociation of the active site. At the same time, the conjugation effect increases the electron cloud density at the active site, which will have a decreasing effect on the degree of dissociation at the active site. Overall, the effectiveness of nitro in activating the active site decreases in the positional order *ortho* > *para* > *meta* [161,267]. Chen et al. introduced *m*-nitrophenyl-O ether into heptacarmine cyanine to synthesize fluorescent probes for detecting H_2S and H_2S_n. Although their probes contained nitrophenyl-O ether groups, the active sites for the reactions with H_2S and H_2S_n were the nitro groups, not the ether bond, and the reaction required 1 h to reach equilibrium [268,269]. Zhang et al. compared the response rates to thiols of three NIR fluorescent probes (Fig. 16, panels **45–2-b**, **45–2-c**, and **45–2-d**) with different detection groups (2,4-dinitrobenzenesulfonate, *o*-nitrobenzenesulfonate, and *p*-nitrobenzenesulfonate), respectively,

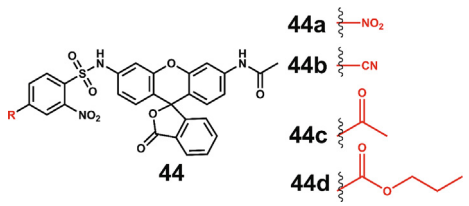

Fig. 15. Comparison of different substituents on the benzene ring (probes 44) [153].

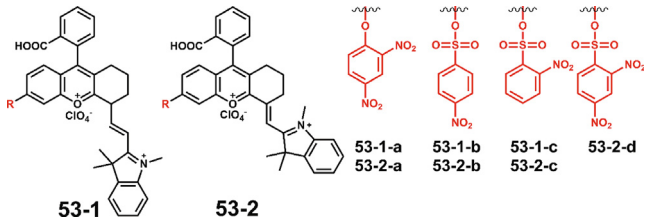

Fig. 16. Comparison of the same fluorophore with different detection groups (probes 45) [267].

and found that the mono-nitro-substituted groups responded more slowly [267].

3.3.3. Effect of the positions of two substituents on the benzene ring

The number of groups appended on the benzene ring will affect the reactivity of the active site [155,161,267]. At present, it is common to introduce doubly-substituted groups, such as 2,4-dinitrophenyl ether, 2,4-dinitrobenzenesulfonamide, 3,5-dinitrophenyl-O ether, 2-fluoro-4-nitrobenzoate, and so on. Taking the 2,4-dinitrophenyl ether group as an example, to maximize the conjugation and induction effects of the electron-withdrawing groups, they are introduced at both the *ortho* and *para* positions of the benzene ring. This arrangement will lower the density of the electron cloud on the benzene ring, which will decrease the bond strength of the reaction site and increase the bond length, so that the reaction site will react more easily [267]. However, the simultaneous introduction of two nitro groups at the *meta* positions of the benzene ring cannot affect the active site through the conjugation effect, and the degree of dissociation is insufficient. Wang et al. appended a 3,5-dinitrophenyl-O ether group on the dicyanoisophorone fluorophore and introduced a formaldehyde group at an *ortho* position of the phenyl-O ether to synthesize a fluorescent probe for detecting H_2S. With phenyl-O ether lacking the *ortho* formaldehyde group, the response of the probe to H_2S was very slow. Introducing the *ortho* formaldehyde group (Michael acceptor) as an auxiliary detection group caused HS^- to induce an initial nucleophilic addition reaction on the aldehyde group, and then reaction of the phenyl-O ether bond eventually formed 3,5-dinitrothiophenol [270]. 2-Fluoro-5-nitrobenzoate is a notable specific group. Theoretically, the response of *m*-nitrobenzoate groups to thiols would be extremely slow; however, the introduction of a fluoro substituent as an auxiliary detection group with an electron-withdrawing effect adjacent to the active site modifies the reactivity of the active site. It facilitates electrophilic reaction with H_2S_n of lower pK_a in preference to the active site, and then another part of unreacted -SH attacks the active site, thereby achieving the purpose of detecting H_2S_n [222,230,271]. Because there are few cases of two different substituents, these are still difficult to discuss.

3.4. Comparison of the same fluorophore with different detection groups

There are many RSS- and RSeS-specific fluorescent probes based on S_NAr reactions, many of which have different detection groups attached to the same fluorophore. Here, we summarize some similar cases and analyze some cases of optimized detection groups.

Dicyanoisophorone is a very popular fluorophore. Because of its simple synthesis, good solubility in water, large Stokes shift, and maximum emission wavelength in the NIR region, it has attracted much attention. Between 2017 and 2019, there were 11 reports concerning the use of dicyanoisophorone as a fluorophore, bearing different electrophilic small aromatic molecules to detect RSS and RSeS (Table 1 and Fig. 17). Three of these reports concerned probe

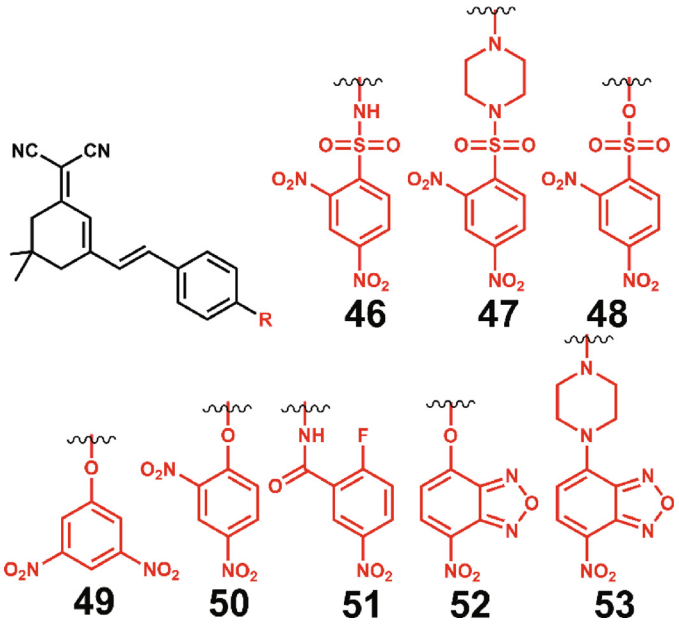

Fig. 17. Comparison of the same fluorophore with different detection groups (probes 46–53) [270–280].

46 (Fig. 17, panel **46**) [272–274], and two concerned probe **47** (Fig. 17, panel **47**) [275,276]. Evidently, 2,4-dinitrobenzenesulfonamide is one of the most commonly used RSS and RSeS detection groups. It can be seen that the response times of the 2,4-dinitrophenyl-O ether (Fig. 17, panel **50**) [277] and 2,4-dinitrobenzenesulfonamide groups are similar, both shorter than that with 2,4-dinitrobenzenesulfonate (Fig. 17, panel **48**) [278]. With the incorporation of piperazine, both nitrogen atoms are reaction sites, thus, the response time is significantly shorter than that with 2,4-dinitrobenzenesulfonimide, and the limit of detection is also lower. However, due to steric hindrance, the rate of reaction of PhSH is significantly slower than that with H_2S. Unfortunately, PhSH has not been included in reported selective experiments on fluorescent probes for H_2S. The 3,5-dinitrophenyl-O ether group (Fig. 17, panel **49**) [270] showed a very slow response to H_2S. Since the NBD group produces different fluorescence emissions when it is incorporated into different structures, NBD-O ether (Fig. 17, panel **52**) [279] can be used for distinguishing between Cys/Hcy and GSH, and the reaction rates with PhSH and H_2S are very slow. The NBD-N group (Fig. 17, panel **53**) [280] incorporating piperazine is more selective for H_2S. The 2-fluoro-5-nitrobenzoate group is very selective for H_2S_n (Fig. 17, panel **51**) [271], but unfortunately there have been no reports on selective experiments on PhSH in the salient literature.

Zhang et al. combined two NIR fluorophores with 2,4-dinitrobenzenesulfonate, *o*-nitrobenzenesulfonate, *p*-nitrobenzenesulfonate, and 2,4-dinitrophenyl-O ether groups, and synthesized seven kinds of fluorescent probes for detecting RSS (Fig. 16) [267]. The selectivity of 2,4-dinitrophenyl-O ether for PhSH, H_2S, and GSH was significantly higher than that of nitrobenzenesulfonate. 2,4-Dinitrobenzenesulfonate showed higher sensitivity than *o*-nitrobenzenesulfonate or *p*-nitrobenzenesulfonate.

Zhao et al. attached different detection groups (*p*-methoxyphenyl, *p*-methylphenyl, phenyl, *p*-trifluoromethylphenyl, *p*-nitrophenyl, or 2,4-dinitrophenyl) to BODIPY fluorophores through secondary amine group, thioether, or oxyether linkages (Fig. 18) [154]. Due to the poor dissociation ability of aromatic amines, all fluorescent probes with aromatic amines as detection groups show almost no reaction with biothiols. All fluorescent probes with phenyl-S ether as the detection group can react with thiols. Appending an electron-withdrawing substituent on the benzene ring enhances the susceptibility of the detection group to cleavage, lowering the selectivity. All fluorescent probes with a phenyl-O ether detection group can respond to thiols. Appending a weakly electron-withdrawing substituent on the benzene ring lowers the susceptibility of the detection group to cleavage, retarding the response to biothiols. After structural optimization, probes containing *p*-methoxyphenyl-S (Fig. 18, panel **54-S-1**) and 2,4-dinitrophenyl-O ether (Fig. 18, panel **54-O-6**) were identified as the most suitable for distinguishing Cys/Hcy and GSH.

Han et al. used naphthalimide as the fluorophore and differently substituted benzenesulfonates as detection groups to screen and synthesize fluorescent probes for detecting GST activity (Fig. 19) [155]. Probes similar to probe **55–1** proved to be ultra-sensitive. By screening different substituents, the non-enzymatic noise of the probe could be greatly reduced, while keeping the sensitivity almost unchanged. For probes **55–11** and **55–12**, the most electrophilic centers were identified as the alternative β-carbon instead of the α-carbon, indicating that they are not suitable as GST detection probes. Probe **55–6** responded slowly to GST with low sensitivity and no background noise at all. It is worth noting that the order of the reaction rates of different probes (**55–2** < **55–4** < **55–3** < **55–5** < **55–1**) is very consistent with the order of the increase rates of fluorescence in non-enzymatic tests. By moderately reducing the sensitivity, probe **55–3** ($\lambda_{ex/em}$ = 445/560-nm) was found to be a more suitable probe. It was also used in more practical and rigorous applications. The limit of detection of this probe for GST was 3.7 nM.

3.5. Introduction of other auxiliary detection groups or bridged small molecules

The introduction of specific functional groups can increase the selectivity of the probe to certain specific RSS or RSeS and accelerate the response rate. Theoretically, the response of *m*-nitrobenzoic acid groups to RSS would be extremely slow. Introducing a fluorine

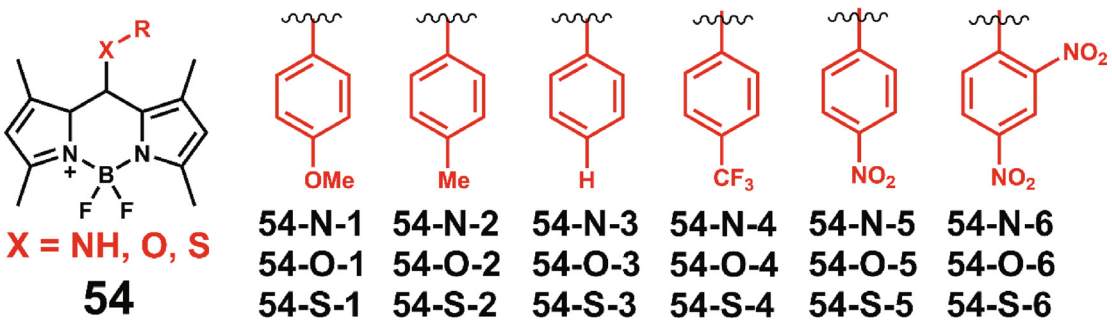

Fig. 18. Comparison of the same fluorophore with different detection groups (probes 54) [154].

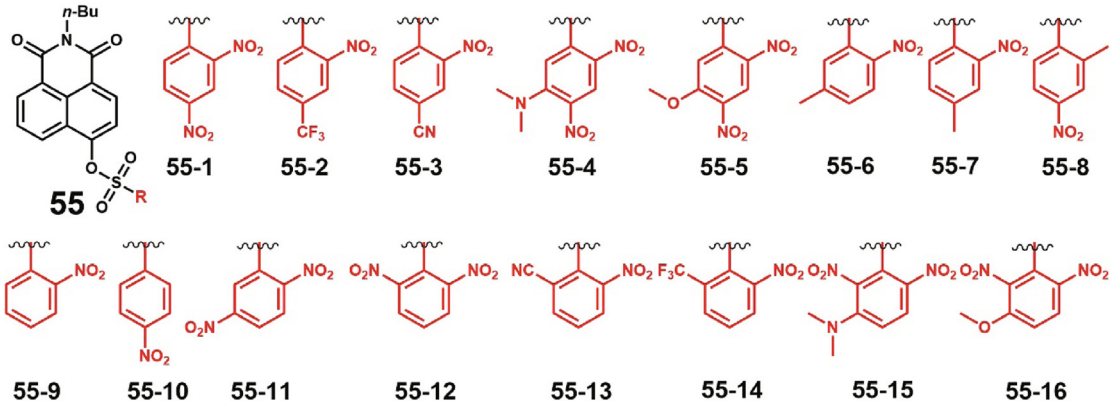

Fig. 19. Comparison of the same fluorophore with different detection groups (probes 55) [155].

atom in the *ortho* position of the *m*-nitrobenzenesulfonate group (the *para* position with respect to the nitro group) improves the selectivity of the probe for H_2S_n, and the greater the number of sulfur atoms, the faster the response [222,230,271]. The 3,5-dinitrophenyl-O ether group responds very slowly to RSS. It is a good choice to introduce a formaldehyde group (Michael acceptor) in the *ortho* position of the fluorophore. The formaldehyde group first reacts with RSS to form activated S^-, and then undergoes S_N-Ar reaction with the phenyl-O ether bond [270]. When the detection group is phenyl-Se ether and a formaldehyde group is introduced adjacent to the detection site of the fluorophore, one GSH molecule can react with two detection groups at the same time, resulting in a more conjugated system, whereas Cys or Hcy can only react with one of the detection groups [103]. The response of 2,4-dinitrophenyl-S to RSS is very slow. The introduction of an *o*-phenyl-S benzoate group between this group and the hydroxyl group in the fluorophore can greatly shorten the RSS response time. When H_2S reacts with the benzoate, O^- is first released to attack the phenyl-S, and then the benzoate and phenyl-S bonds are successively broken; the hydroxyl group on the fluorophore is exposed to achieve H_2S detection [281–283]. Of course, introducing a piperazine group between the detection group and the fluorophore increases the number of reaction sites, and hence the sensitivity to the analyte, and the reaction equilibrium time is greatly shortened [250,275,276]. In addition, the introduction of selenophenol at the ortho position of the benzoate can make the selenophenol form a selenium-sulfur bond with highly active thiols, thereby causing internal cyclization to break the benzoate, which has achieved the purpose of detecting sulfane sulfur [225,228].

3.6. S_NAr-based fluorescent probe for RSeS

To date, most RSeS probes based on S_NAr reactions have been designed by simulating RSS probes. 2,4-Dinitrophenyl-O ether and 2,4-dinitrobenzenesulfonamide have mainly been used as detection groups, but 2,4-dinitrobenzenesulfonate is not strong in distinguishing RSeS and RSS [129,267]. However, in order to avoid the interference of thiols as far as possible, rational selection of the detection group is only one aspect. The pH of the detection environment is another aspect. Cys-SH has a pK_a of 8.5 and Sec-SeH has a pK_a of 5.2. In physiological systems, Se in selenol decomposes into R-Se^-, which is more reactive than a thiol, whereas S in thiol exists in the form of undecomposed R-SH. Therefore, R-SeH can be selectively probed over R-SH in an acidic environment [146]. Hatsuo et al. proved that 3′-(2,4-dinitrobenzenesulfonyl)-2′,7′-dimethylfluorescein (BESThio, Fig. 1, panel **1b**) has a dual ability to detect selenol in an acidic environment and thiol under neutral or alkaline conditions [135,136]. This is not only due to the different pK_a values of R-SeH and R-SH, but also because selenol has stronger nucleophilicity than thiol.

4. Conclusions and outlook

In this review, we have described a series of fluorescent probes based on S_NAr reaction for the specific detection of RSS and RSeS, and have classified them according to their reaction mechanisms. The mechanism of detecting RSS and RSeS is reliant on the strong nucleophilicity of thiol and selenol, as a result of which an aromatic detection group is displaced, thereby modifying the fluorescence of the probe [129,136]. Benzenesulfonate, phenyl-O ether, phenyl-S ether, phenyl-Se ether, 7-nitro-2,1,3-benzoxadiazole, benzoate, and a selenium-nitrogen bond are all good detection groups [44–48]. All of the probes discussed herein exhibit excellent optical performance upon reaction with the target analytes and represent powerful tools for the direct detection of RSS and RSeS.

When designing a fluorescent probe based on an S_NAr reaction, the main factors affecting the selectivity to RSS and RSeS are the reactivity of the site at which the substitution occurs, and the nature, number, and positions of substituents on the detection group. An ether linkage is a popular reaction site. The ease of dissociation of an ether increases with the increasing atomic radii of O, S, and Se. Due to the inherently low degree of dissociation of a phenyl-O ether group, although a phenyl-O linkage moiety bearing a single substituent can respond to RSS and RSeS, the response times are too long and the selectivity is poor [161]. More popular phenyl-O ether groups are those bearing two substituents, which show shorter response times to RSS and RSeS and improved selectivity, most notably the 2,4-dinitrophenyl-O ether group [162–166]. The phenyl-O ether group itself can respond to RSS and RSeS, but it does not have a quenching effect, so it is not very suitable for detection [161]. The quenching effect of phenyl-O ether groups is mainly dependent on the substituents on the benzene ring, so the selectivity for RSS and RSeS depends more on the detection environment and the pK_a of the analyte. The degree of dissociation of the phenyl-S ether group is moderate. Generally, the introduction of appropriate substituents at the *ortho* and/or *para* positions of the benzene ring can impart a response to RSS. At the same time, because the covalent bond with sulfur produces a quenching effect, detection does not depend on the substituent. After displacement of the detection group, the analyte combines with the fluorophore, so it is more suitable for distinguishing RSS with different structures, but similar pK_a values [100,101]. Of course, RSS with higher pK_a can also be detected. However, the sulfur atom is intrinsically

susceptible to interference from ROS, modifying the fluorescence of the probe [178]. There have been few studies on RSS probes employing phenyl-Se ether as the detection group, but we have gratifyingly found that phenyl-Se ether can detect RSS without any substituent on the benzene ring [103,104]. However, selenium atoms are more susceptible to interference from ROS than sulfur atoms, eliciting fluorescence changes [190,260,261]. Benzenesulfonamide has a lower degree of dissociation and higher selectivity than benzenesulfonate, so it is suitable for detecting RSS and RSeS with lower pK_a values [129]. The influence of substituents on the benzene ring also follows the above rules. 2,4-Dinitrobenzenesulfonamide and 2,4-dinitrobenzenesulfonate are the two most commonly used detection groups. Since the NBD group is modified upon analyte-induced dissociation, it produces different fluorescence emissions [208,209]. Therefore, NBD-O ether can be used to distinguish RSS with different structures but similar pK_a values [210,211]. Thiolysis of the NBD-N group is H_2S-specific, and may be exploited for the development of highly selective fluorescent probes and scavengers for H_2S. The active sites of benzoates mainly simulate NCL reaction [221,222]. In fact, regardless of whether the detection site is thiobenzoate or benzoate, the test substance always forms a new thiolipid with the carboxyl group. For benzoate esters, the exposure of hydroxyl groups of the fluorophore occurs concomitantly with the combination of RSS and benzoic acid [221,229]. For the active sites of thiobenzoates, due to the powerful quenching effect of sulfur atoms, the thiophenol-containing groups are always displaced, and the fluorophores combine with the analyte to produce fluorescence at different emission wavelengths. Therefore, RSS probes with thiobenzoate as the active site are suitable for distinguishing RSS with different structures based on the ratio of their fluorescences [231,232,235]. Interestingly, the same type of detection group responds more rapidly to RSeS than to RSS. Larger conjugated systems or more stable detection groups or active sites can be used to detect RSS with lower pK_a or even RSeS [129]. Some selenium-containing fluorescent probes based on S_NAr reaction have not been considered as fluorescent probes for detecting RSeS, but may be potentially useful for this purpose [76,77,284]. The introduction of RSS reactive groups (such as Michael acceptors, disulfide bond compounds, etc.) following other mechanisms in the vicinity of the active site (whether fluorophore or detection group) is beneficial for improving the reactivity at this site and the selectivity for the test substance [103,230,270,285]. Bridging the fluorophore and detection group with piperidine has been shown to be helpful for improving the sensitivity of the tested substance and greatly shortens the detection time [250]. In fact, there are many aromatic groups that can be combined with fluorophores and attacked by RSS or RSeS in an S_N-Ar fashion [243,244,286]. Some probes containing aromatic groups for detecting ROS or RNS are also potential tools for detecting RSS or RSeS.

The international enthusiasm for developing RSS and RSeS fluorescent probes based on S_NAr reactions is very high. Despite significant progress in this area, there are still some challenges that require further research in the design and application of probes. Thus, (1) inexpensive, highly emissive, and highly stable fluorophores are still urgently needed. (2) The development of new sensing mechanisms is crucial, not limited to S_NAr. Indeed, S_NAr is just a common reaction mechanism inspired by classical organic synthesis literature and various natural products with thiol or selenol inhibitors. (3) Due to the different concentrations of RSS and RSeS in biological environments, the sensing mechanism should be carefully considered when detecting different analytes at the same time. Meanwhile, the influence of the cell microenvironment on the response characteristics of the probe cannot be ignored. (4) In testing certain specific biological samples, it is necessary to fully evaluate the key point of application, such as biological significance, test results visible to the naked eye, test speed, and so on. (5) RSeS is more active than RSS in anti-oxidation, maintaining physiological balance. The demand for RSeS probes operating under physiological conditions is urgent. We hope that high-level research in this area will continue, and eventually provide tools that can image and measure RSS and RSeS concentrations with high accuracy and reproducibility. Multidisciplinary intersection and wide application is the trend in this field. We should cooperate with biologist, environmental protection scholars, food industry employees, and clinical experts to design and develop tools in a way that is useful and applicable to these users. Only then can we generate new biological knowledge through the detection of RSS and RSeS to better understand, diagnose, monitor, and treat diseases.

Declaration of Competing Interest

The authors declare that they have no known competing financial interests or personal relationships that could have appeared to influence the work reported in this paper.

Acknowledgments

This study was supported by the National Natural Science Foundation of China (31802073), the Special Basic Research Fund for Central Public Research Institutes (Y2020PT19), the Chinese Academy of Agricultural Science and Technology Innovation Project (ASTIP-IAS-12), the Special Basic Research Fund for Central Public Research Institutes (2019-YWF-YB-01) and the Key Laboratory of Se-enriched Products Development and Quality Control, Ministry of Agriculture and Rural Affairs/National-Local Joint Engineering Laboratory of Se-enriched Food Development (Se-2018HZ01).

Appendix A. Supplementary data

Supplementary data to this article can be found online at https://doi.org/10.1016/j.ccr.2020.213601.

References

[1] C. Jacob, G.I. Giles, N.M. Giles, H. Sies, Angew. Chem. Int. Ed. 42 (2003) 4742–4758.
[2] M.J. Long, J.R. Poganik, S. Ghosh, Y. Aye, ACS Chem.Biol. 12 (2017) 586–600.
[3] X. Chen, Y. Zhou, X. Peng, J. Yoon, Chem. Soc. Rev. 39 (2010) 2120–2135.
[4] V.S. Lin, W. Chen, M. Xian, C.J. Chang, Chem. Soc. Rev. 44 (2015) 4596–4618.
[5] S. Ding, M. Liu, Y. Hong, Sci. China Chem. 61 (2018) 882–891.
[6] Z. Xu, T. Qin, X. Zhou, L. Wang, B. Liu, Trend, Anal. Chem. 121 (2019) 115672–115683.
[7] Y. Liu, X. Feng, Y. Yu, Q. Zhao, C. Tang, J. Zhang, Anal. Chim. Acta 1110 (2020) 141–150.
[8] D. Wu, L. Chen, N. Kwon, J. Yoon, Chem 1 (2016) 674–698.
[9] R. Mousa, R. Notis Dardashti, N. Metanis, Angew. Chem. Int. Ed. 56 (2017) 15818–15827.
[10] R.N. Dardashti, L. Dery, R. Mousa, S. Dery, P.S. Reddy, N. Metanis, The chemistry of selenocysteine in proteins, in: D.L. Hatfield, U. Schweizer, P.A. Tsuji, V.N. Gladyshev (Eds.), Selenium: Its Molecular Biology and Role in Human Health, Springer International Publishing, Cham, 2016, pp. 73–83.
[11] M. Kieliszek, S. Blazejak, Molecules 21 (2016) 609–625.
[12] E.E. Schmidt, E.S.J. Arnér, Thioredoxin reductase 1 as an anticancer drug target, in: D.L. Hatfield, U. Schweizer, P.A. Tsuji, V.N. Gladyshev (Eds.), Selenium: Its Molecular Biology and Role in Human Health, Springer International Publishing, Cham, 2016, pp. 199–209.
[13] U. Schweizer, L. Schomburg, J. Köhrle, Selenoprotein P and selenium distribution in mammals, in: D.L. Hatfield, U. Schweizer, P.A. Tsuji, V.N. Gladyshev (Eds.), Selenium: Its Molecular Biology and Role in Human Health, Springer International Publishing, Cham, 2016, pp. 261–274.
[14] L. Turell, R. Radi, B. Alvarez, Free Radical Biol. Med. 65 (2013) 244–253.
[15] L. White, S. Castellano, The role of selenium in human evolution, in: D.L. Hatfield, U. Schweizer, P.A. Tsuji, V.N. Gladyshev (Eds.), Selenium: Its Molecular Biology and Role in Human Health, Springer International Publishing, Cham, 2016, pp. 59–71.
[16] J. Zhang, X. Chai, X.P. He, H.J. Kim, J. Yoon, H. Tian, Chem. Soc. Rev. 48 (2019) 683–722.

[17] G. Giles, Free Radical Biol. Med. 31 (2001) 1279–1283.
[18] G.F. Combs Jr., Nutrients 7 (2015) 2209–2236.
[19] L. Schomburg, Human clinical trials involving selenium, in: D.L. Hatfield, U. Schweizer, P.A. Tsuji, V.N. Gladyshev (Eds.), Selenium: Its Molecular Biology and Role in Human Health, Springer International Publishing, Cham, 2016, pp. 307–319.
[20] N. Kwon, Y. Hu, J. Yoon, ACS Omega 3 (2018) 13731–13751.
[21] Y. Yue, F. Huo, F. Cheng, X. Zhu, T. Mafireyi, R.M. Strongin, C. Yin, Chem. Soc. Rev. 48 (2019) 4155–4177.
[22] R. Zhang, J. Yong, J. Yuan, Z. Ping Xu, Coordin. Chem. Rev. 408 (2020) 213182–213223.
[23] K.M. Reddy, G. Mugesh, Chem.-Eur. J. 25 (2019) 8875–8883.
[24] W.H. Habig, M.J. Pabst, W.B. Jakoby, J. Biol. Chem. 249 (1974) 7130–7139.
[25] A. Wahllander, H. Sies, Eur. J. Biochem. 96 (1979) 441–446.
[26] D.T. Lincoln, E.M.A. Emadi, K.F. Tonissen, F.M. Clarke, Anticancer Res. 23 (2002) 2425–2433.
[27] D.T. Lincoln, F. Al-Yatama, F.M. Mohammed, A.G. Al-Banaw, M. Al-Bader, M. Burge, F. Sinowatz, P.K. Singal, Anticancer Res. 30 (2010) 767–775.
[28] Y. Soini, K. Kahlos, U. Napankangas, R. Kaarteenaho-Wiik, M. Saily, P. Koistinen, P. Paaakko, A. Holmgren, V.L. Kinnula, Clin. Cancer Res. 7 (2001) 1750–1757.
[29] B. Uttara, A.V. Singh, P. Zamboni, R.T. Mahajan, Curr. Neuropharmacol. 7 (2009) 65–74.
[30] R.B. Stricker, Y.S. Zhu, B.F. Elswood, C. Dumlao, J. Van Elk, T.G. Berger, J. Tappero, W.L. Epstein, D.D. Kiprov, Immunol. Lett. 36 (1993) 1–6.
[31] E.S.J. Arnér, M. Björnstedt, A. Holmgren, J. Biol. Chem. 270 (1995) 3479–3482.
[32] C.H. Lillig, A. Holmgren, Antioxid. Redox. Sign. 9 (2007) 25–47.
[33] A. Holmgren, J. Lu, Biochem. Biophys. Res. Commun. 396 (2010) 120–124.
[34] D. Mustacich, G. Powis, Biochem. J. 346 (2000) 1–8.
[35] J. Nordberg, L. Zhong, A. Holmgren, E.S.J. Arner, J. Biol. Chem. 273 (1998) 10835–10842.
[36] K. Anestål, E.S.J. Arnér, J. Biol. Chem. 278 (2003) 15966–15972.
[37] J. Zhang, X. Li, X. Han, R. Liu, J. Fang, Trends Pharmacol. Sci. 38 (2017) 794–808.
[38] M.H. Yoo, X.M. Xu, B.A. Carlson, A.D. Patterson, V.N. Gladyshev, D.L. Hatfield, PloS one 2 (2007) e1112–e1119.
[39] J. Lu, E.H. Chew, A. Holmgren, Proc. Natl. Acad. Sci. U. S. A. 104 (2007) 12288–12293.
[40] T.C. Karlenius, K.F. Tonissen, Cancers 2 (2010) 209–232.
[41] G. Powis, D.L. Kirkpatrick, Curr. Opin. Pharmacol. 7 (2007) 392–397.
[42] T. Tamura, T.C. Stadtman, Proc. Natl. Acad. Sci. U. S. A. 93 (1996) 1006–1011.
[43] E.S. Arner, A. Holmgren, Eur. J. Biochem. 267 (2000) 6102–6109.
[44] H.S. Jung, X. Chen, J.S. Kim, J. Yoon, Chem. Soc. Rev. 42 (2013) 6019–6031.
[45] L.Y. Niu, Y.Z. Chen, H.R. Zheng, L.Z. Wu, C.H. Tung, Q.Z. Yang, Chem. Soc. Rev. 44 (2015) 6143–6160.
[46] B. Thomas, K.C. Yan, X.L. Hu, M. Donnier-Marechal, G.R. Chen, X.P. He, S. Vidal, Chem. Soc. Rev. 49 (2020) 593–641.
[47] W. Sun, S. Guo, C. Hu, J. Fan, X. Peng, Chem. Rev. 116 (2016) 7768–7817.
[48] L.M. Hyman, K.J. Franz, Coordin. Chem. Rev. 256 (2012) 2333–2356.
[49] Y. Gao, J. Zhang, X. Kang, China Med. Device Inf. 23 (2017) 18–21.
[50] L.I. Jiajie, L.I. Nan, Y. Ren, S. Chen, Food Sci. 37 (2016) 283–288.
[51] W.-D. Guan, L.-P. Chen, F. Ye, D. Ye, S.-G. Wu, H.-X. Zhou, J.-Y. He, C.-G. Yang, Z.-Q. Zeng, Y.-T. Wang, Chin. Med. J., 133 (2020) E019-E019.
[52] S.S. Babu, V.K. Praveen, A. Ajayaghosh, Chem. Rev. 114 (2014) 1973–2129.
[53] D. Cao, Z. Liu, P. Verwilst, S. Koo, P. Jangjili, J.S. Kim, W. Lin, Chem. Rev. 119 (2019) 10403–10519.
[54] X. Li, X. Gao, W. Shi, H. Ma, Chem. Rev. 114 (2014) 590–659.
[55] K.Y. Zhang, Q. Yu, H. Wei, S. Liu, Q. Zhao, W. Huang, Chem. Rev. 118 (2018) 1770–1839.
[56] J. Wang, H.-B. Liu, Z. Tong, C.-S. Ha, Coordin Chem. Rev. 303 (2015) 139–184.
[57] A.P. de Silva, Nat. Chem. 4 (2012) 440–441.
[58] T. Ueno, T. Nagano, Nat. Methods 8 (2011) 642–645.
[59] D.J. Arndt-Jovin, M. Robert-Nicoud, S.J. Kaufman, T.M. Jovin, Science 230 (1985) 247–256.
[60] X. Han, X. Song, F. Yu, L. Chen, Adv. Funct. Mater. 27 (2017) 1700769–1700778.
[61] F. Kong, Y. Zhao, Z. Liang, X. Liu, X. Pan, D. Luan, K. Xu, B. Tang, Anal. Chem. 89 (2017) 688–693.
[62] D. Luan, X. Gao, F. Kong, X. Song, A. Zheng, X. Liu, K. Xu, B. Tang, Anal. Chem. 90 (2018) 9523–9528.
[63] P. Gao, W. Pan, N. Li, B. Tang, Chem. Sci. 10 (2019) 6035–6071.
[64] X. Pan, X. Song, C. Wang, T. Cheng, D. Luan, K. Xu, B. Tang, Theranostics 9 (2019) 1794–1808.
[65] X. Han, X. Song, F. Yu, L. Chen, Chem. Sci. 8 (2017) 6991–7002.
[66] B. Zhang, Y. Liu, X. Li, J. Xu, J. Fang, Chem.-Asian J. 13 (2018) 3593–3600.
[67] B. Zhang, J. Zhang, S. Peng, R. Liu, X. Li, Y. Hou, X. Han, J. Fang, Expert Opin. Ther. Pat. 27 (2017) 547–556.
[68] L. Strekowski, M. Lipowska, G. Patonay, J. Org. Chem. 57 (1992) 4578–4580.
[69] N. Kaur, S. Chopra, G. Singh, P. Raj, A. Bhasin, S.K. Sahoo, A. Kuwar, N. Singh, J. Mater. Chem. B 6 (2018) 4872–4902.
[70] S. Lee, J. Li, X. Zhou, J. Yin, J. Yoon, Coordin. Chem. Rev. 366 (2018) 29–68.
[71] D. Amilan Jose, N. Sharma, R. Sakla, R. Kaushik, S. Gadiyaram, Methods 168 (2019) 62–75.
[72] L. Yi, Z. Xi, Org. Biomol. Chem. 15 (2017) 3828–3839.
[73] M. Gao, B.Z. Tang, ACS Sensors 2 (2017) 1382–1399.
[74] B.J. Bezner, L.S. Ryan, A.R. Lippert, Anal. Chem. 92 (2020) 309–326.
[75] X. Jiao, Y. Li, J. Niu, X. Xie, X. Wang, B. Tang, Anal. Chem. 90 (2018) 533–555.
[76] Z. Lou, P. Li, K. Han, Accounts Chem. Res. 48 (2015) 1358–1368.
[77] S.T. Manjare, Y. Kim, D.G. Churchill, Accounts Chem. Res. 47 (2014) 2985–2998.
[78] W. Chyan, R.T. Raines, ACS Chem.Biol. 13 (2018) 1810–1823.
[79] K. Singh, A.M. Rotaru, A.A. Beharry, ACS Chem.Biol. 13 (2018) 1785–1798.
[80] S.P. Wang, W.J. Deng, D. Sun, M. Yan, H. Zheng, J.G. Xu, Org. Biomol. Chem. 7 (2009) 4017–4020.
[81] K. Cui, Z. Chen, Z. Wang, G. Zhang, D. Zhang, Analyst 136 (2011) 191–195.
[82] H. Guo, Y. Jing, X. Yuan, S. Ji, J. Zhao, X. Li, Y. Kan, Org. Biomol. Chem. 9 (2011) 3844–3853.
[83] M. Lan, J. Wu, W. Liu, H. Zhang, W. Zhang, X. Zhuang, P. Wang, Sens. Actuat. B 156 (2011) 332–337.
[84] J. Shao, H. Guo, S. Ji, J. Zhao, Biosens. Bioelectron. 26 (2011) 3012–3017.
[85] J. Bouffard, Y. Kim, T.M. Swager, R. Weissleder, S.A. Hilderbrand, Org. Lett. 10 (2008) 37–40.
[86] S. Ji, J. Yang, Q. Yang, S. Liu, M. Chen, J. Zhao, J. Org. Chem. 74 (2009) 4855–4865.
[87] J. Li, C.F. Zhang, S.H. Yang, W.C. Yang, G.F. Yang, Anal. Chem. 86 (2014) 3037–3042.
[88] D. Yu, F. Huang, S. Ding, G. Feng, Anal. Chem. 86 (2014) 8835–8841.
[89] T. Liu, Z. Xu, D.R. Spring, J. Cui, Org. Lett. 15 (2013) 2310–2313.
[90] T. Liu, X. Zhang, Q. Qiao, C. Zou, L. Feng, J. Cui, Z. Xu, Dyes Pigments 99 (2013) 537–542.
[91] Z. Dai, L. Tian, B. Song, Z. Ye, X. Liu, J. Yuan, Anal. Chem. 86 (2014) (1889) 11883–11891.
[92] Z. Huang, S. Ding, D. Yu, F. Huang, G. Feng, Chem. Commun. 50 (2014) 9185–9187.
[93] H.-Y. Liu, M. Zhao, Q.-L. Qiao, H.-J. Lang, J.-Z. Xu, Z.-C. Xu, Chinese Chem. Lett. 25 (2014) 1060–1064.
[94] Y. Liu, G. Feng, Org. Biomol. Chem. 12 (2014) 438–445.
[95] D. Maity, A. Raj, P.K. Samanta, D. Karthigeyan, T.K. Kundu, S.K. Pati, T. Govindaraju, RSC Adv. 4 (2014) 11147–11151.
[96] I. Simsek Turan, F. Sozmen, Sens. Actuat. B, 201 (2014) 13-18.
[97] C. Tang, Q. Zheng, S. Zong, Z. Wang, Y. Cui, Sens. Actuat. B 202 (2014) 99–104.
[98] L. Yuan, Q.-P. Zuo, Sens. Actuat. B 196 (2014) 151–155.
[99] Y.-S. Guan, L.-Y. Niu, Y.-Z. Chen, L.-Z. Wu, C.-H. Tung, Q.-Z. Yang, RSC Adv. 4 (2014) 8360–8364.
[100] L.-Y. Niu, Q.-Q. Yang, H.-R. Zheng, Y.-Z. Chen, L.-Z. Wu, C.-H. Tung, Q.-Z. Yang, RSC Adv. 5 (2015) 3959–3964.
[101] L. Song, Q. Sun, N. Wang, Z. Chen, W. Zhang, J. Qian, Anal. Methods 7 (2015) 10371–10375.
[102] L. Song, H. Tian, X. Pei, Z. Zhang, W. Zhang, J. Qian, RSC Adv. 5 (2015) 59056–59061.
[103] Y. Kim, S.V. Mulay, M. Choi, S.B. Yu, S. Jon, D.G. Churchill, Chem. Sci. 6 (2015) 5435–5439.
[104] D. Gong, X. Zhu, Y. Tian, S.C. Han, M. Deng, A. Iqbal, W. Liu, W. Qin, H. Guo, Anal. Chem. 89 (2017) 1801–1807.
[105] C. Wei, L. Wei, Z. Xi, L. Yi, Tetrahedron Lett. 54 (2013) 6937–6939.
[106] C. Zhang, L. Wei, C. Wei, J. Zhang, R. Wang, Z. Xi, L. Yi, Chem. Commun. 51 (2015) 7505–7508.
[107] J. Bae, J. Choi, T.J. Park, S.-K. Chang, Tetrahedron Lett. 55 (2014) 1171–1174.
[108] M.D. Hammers, M.D. Pluth, Anal. Chem. 86 (2014) 7135–7140.
[109] C. Wei, Q. Zhu, W. Liu, W. Chen, Z. Xi, L. Yi, Org. Biomol. Chem. 12 (2014) 479–485.
[110] L.A. Montoya, T.F. Pearce, R.J. Hansen, L.N. Zakharov, M.D. Pluth, J. Org. Chem. 78 (2013) 6550–6557.
[111] J. Wang, Y. Liao, S. Shao, Chem. Lett. 44 (2015) 1437–1439.
[112] L. Fan, W. Zhang, X. Wang, W. Dong, Y. Tong, C. Dong, S. Shuang, Analyst 144 (2019) 439–447.
[113] C.-S. Jiang, Z.-Q. Cheng, Y.-X. Ge, J.-L. Song, J. Zhang, H. Zhang, Anal. Methods 11 (2019) 3736–3740.
[114] W. Lv, Y. Chen, L. Bian, X. Chen, Talanta 197 (2019) 204–210.
[115] C. Wang, Y. Wang, G. Wang, S. Chen, C. Huang, J. Mater. Chem. B 7 (2019) 5633–5639.
[116] H. Yan, Y. Yue, C. Yin, Y. Zhang, J. Chao, F. Huo, Spectrochim. Acta A 229 (2020) 117905–117911.
[117] S. Pagidi, N.K. Kalluvettukuzhy, P. Thilagar, Langmuir 34 (2018) 8170–8177.
[118] J. Wu, Z. Ye, F. Wu, H. Wang, L. Zeng, G.M. Bao, Talanta 181 (2018) 239–247.
[119] S. Feng, Q. Xia, G. Feng, Dyes Pigments 163 (2019) 447–453.
[120] J. Wu, D. Su, C. Qin, W. Li, J. Rodrigues, R. Sheng, L. Zeng, Talanta 201 (2019) 111–118.
[121] Y. Wang, L. Wang, E. Jiang, M. Zhu, Z. Wang, S. Fan, Q. Gao, S. Liu, Q.X. Li, R. Hua, Dyes Pigments 156 (2018) 338–347.
[122] B. Yang, M.-M. Su, Y.-S. Xue, Z.-X. He, C. Xu, H.-L. Zhu, Sens. Actuat. B 276 (2018) 456–465.
[123] H. Zhang, M. Li, W. Feng, G. Feng, Dyes Pigments 149 (2018) 475–480.
[124] P. Zhang, Y. Ding, W. Liu, G. Niu, H. Zhang, J. Ge, J. Wu, Y. Li, P. Wang, Sens. Actuat. B 264 (2018) 234–239.
[125] D. Cheng, Y. Pan, B.-C. Yin, L. Yuan, X.-B. Zhang, Chinese Chem. Lett. 28 (2017) 1987–1990.
[126] M.G. Choi, M.J. Cho, H. Ryu, J. Hong, S.-K. Chang, Dyes Pigments 143 (2017) 123–128.
[127] W. Feng, M. Li, Y. Sun, G. Feng, Anal. Chem. 89 (2017) 6106–6112.
[128] H. Shang, H. Chen, Y. Tang, Y. Ma, W. Lin, Biosens. Bioelectron. 95 (2017) 81–86.

[129] B. Zhang, C. Ge, J. Yao, Y. Liu, H. Xie, J. Fang, J. Am. Chem. Soc. 137 (2015) 757–769.
[130] H. Chen, B. Dong, Y. Tang, W. Lin, Chem.-Eur. J. 21 (2015) 11696–11700.
[131] S. Areti, S.K. Verma, J. Bellare, C.P. Rao, Anal. Chem. 88 (2016) 7259–7267.
[132] Q. Sun, S.H. Yang, L. Wu, Q.J. Dong, W.C. Yang, G.F. Yang, Anal. Chem. 88 (2016) 6084–6091.
[133] Q. Sun, S.H. Yang, L. Wu, W.C. Yang, G.F. Yang, Anal. Chem. 88 (2016) 2266–2272.
[134] W. Zhang, F. Huo, T. Liu, Y. Wen, C. Yin, Dyes Pigments 133 (2016) 248–254.
[135] H. Maeda, H. Matsuno, M. Ushida, K. Katayama, K. Saeki, N. Itoh, Angew. Chem. Int. Ed. 44 (2005) 2922–2925.
[136] H. Maeda, K. Katayama, H. Matsuno, T. Uno, Angew. Chem. Int. Ed. 45 (2006) 1810–1813.
[137] J. Wang, H. Wang, Y. Hao, S. Yang, H. Tian, B. Sun, Y. Liu, Food Chem. 262 (2018) 67–71.
[138] Z. Dai, L. Tian, Z. Ye, B. Song, R. Zhang, J. Yuan, Anal. Chem. 85 (2013) 11658–11664.
[139] Y. Nan, W. Zhao, X. Xu, C.-T. Au, R. Qiu, RSC Adv. 5 (2015) 69299–69306.
[140] P. Zhang, Y. Hong, H. Wang, M. Yu, Y. Gao, R. Zeng, Y. Long, J. Chen, Polym. Chem. 8 (2017) 7271–7278.
[141] G. Jiang, X. Liu, Q. Chen, G. Zeng, Y. Wu, X. Dong, G. Zhang, Y. Li, X. Fan, J. Wang, Sens. Actuat. B 252 (2017) 712–716.
[142] W. Jiang, Q. Fu, H. Fan, J. Ho, W. Wang, Angew. Chem. Int. Ed. 46 (2007) 8445–8448.
[143] S. Zhang, Q. Wang, X. Liu, J. Zhang, X.F. Yang, Z. Li, H. Li, Anal. Chem. 90 (2018) 4119–4125.
[144] X. Han, R. Wang, X. Song, F. Yu, L. Chen, Anal. Chem. 90 (2018) 8108–8115.
[145] G. Liao, F. He, Q. Li, L. Zhong, R. Zhao, H. Che, H. Gao, B. Fang, Prog. Mater. Sci. 112 (2020) 100666–100687.
[146] Q. Wang, S. Zhang, Y. Zhong, X.F. Yang, Z. Li, H. Li, Anal. Chem. 89 (2017) 1734–1741.
[147] C.-G. Dai, J.-L. Wang, Q.-H. Song, J. Mater. Chem. B 4 (2016) 6726–6733.
[148] Q. Ma, J. Xu, X. Zhang, L. Zhou, H. Liu, J. Zhang, Sens. Actuat. B 229 (2016) 434–440.
[149] S. Chen, H. Li, P. Hou, Anal. Chim. Acta 993 (2017) 63–70.
[150] W. Chen, X. Yue, W. Li, Y. Hao, L. Zhang, L. Zhu, J. Sheng, X. Song, Sens. Actuat. B 245 (2017) 702–710.
[151] L.Y. Niu, Y.S. Guan, Y.Z. Chen, L.Z. Wu, C.H. Tung, Q.Z. Yang, Chem. Commun. 49 (2013) 1294–1296.
[152] S. Zhang, F. Cai, B. Hou, H. Chen, C. Gao, X.-C. Shen, H. Liang, New J. Chem. 43 (2019) 6696–6701.
[153] A. Shibata, Y. Nakano, M. Ito, M. Araki, J. Zhang, Y. Yoshida, S. Shuto, B. Mannervik, R. Morgenstern, Y. Ito, H. Abe, Analyst 138 (2013) 7326–7330.
[154] J. Zhang, X. Ji, H. Ren, J. Zhou, Z. Chen, X. Dong, W. Zhao, Sens. Actuat. B 260 (2018) 861–869.
[155] X.X. Zhang, H. Qi, M.H. Lu, S.Q. Yang, P. Li, H.L. Piao, K.L. Han, Research 2020 (2020) 7043124–7043135.
[156] X.-B. Wang, X. Hao, D. Zhang, Y. Jiang, Dyes Pigments 142 (2017) 167–174.
[157] B. Gu, W. Su, L. Huang, C. Wu, X. Duan, Y. Li, H. Xu, Z. Huang, H. Li, S. Yao, Sens. Actuat. B 255 (2018) 2347–2355.
[158] S.H. Guo, T.H. Leng, K. Wang, C.Y. Wang, Y.J. Shen, W.H. Zhu, Talanta 185 (2018) 359–364.
[159] U.N. Guria, K. Maiti, S.S. Ali, S.K. Samanta, D. Mandal, R. Sarkar, P. Datta, A.K. Ghosh, A.K. Mahapatra, New J. Chem. 42 (2018) 5367–5375.
[160] K. Pal, A.S.M. Islam, C. Prodhan, S. Bhunya, A. Paul, M. Ali, ChemistrySelect 3 (2018) 7283–7290.
[161] X. Wang, J. Lv, X. Yao, Y. Li, F. Huang, M. Li, J. Yang, X. Ruan, B. Tang, Chem. Commun. 50 (2014) 15439–15442.
[162] Z. Yao, W. Ge, M. Guo, K. Xiao, Y. Qiao, Z. Cao, H.C. Wu, Talanta 185 (2018) 146–150.
[163] B. Yu, C. Chen, J. Ru, W. Luo, W. Liu, Talanta 188 (2018) 370–377.
[164] S. Zhou, Y. Rong, H. Wang, X. Liu, L. Wei, X. Song, Sens. Actuat. B 276 (2018) 136–141.
[165] T. Fang, X.-D. Jiang, C. Sun, Q. Li, Sens. Actuat. B 290 (2019) 551–557.
[166] X. Lin, X. Lu, J. Zhou, H. Ren, X. Dong, W. Zhao, Z. Chen, Spectrochim. Acta A 213 (2019) 416–422.
[167] R. Ren, H.C. Xu, H. Dong, H.T. Peng, P.P. Wu, Y. Qiu, S.G. Yang, Q. Sun, N.F. She, Talanta 205 (2019) 120067–120077.
[168] L. Yang, Y. Liu, Y. Li, H. Wang, H. Zhang, J. Xu, L. Ji, Q. Wang, G. He, Tetrahedron 75 (2019) 130538–130544.
[169] H. Zhang, L. Xu, W. Li, W. Chen, Q. Xiao, J. Huang, C. Huang, J. Sheng, X. Song, RSC Adv. 9 (2019) 7955–7960.
[170] D. Su, D. Cheng, Y. Lv, X. Ren, Q. Wu, L. Yuan, Spectrochim. Acta A 226 (2020) 117635–117642.
[171] M. Li, W. Feng, Q. Zhai, G. Feng, Biosens. Bioelectron. 87 (2017) 894–900.
[172] N. Li, A. Than, J. Chen, F. Xi, J. Liu, P. Chen, Biomater. Sci. 6 (2018) 779–784.
[173] L. Sun, Y. Wu, J. Chen, J. Zhong, F. Zeng, S. Wu, Theranostics 9 (2019) 77–89.
[174] P. Zhang, X. Nie, M. Gao, F. Zeng, A. Qin, S. Wu, B.Z. Tang, Mater. Chem. Front. 1 (2017) 838–845.
[175] Y. Liu, X. Lv, J. Liu, Y.Q. Sun, W. Guo, Chem.-Eur. J. 21 (2015) 4747–4754.
[176] Y. Tang, L. Jin, B. Yin, Anal. Chim. Acta 993 (2017) 87–95.
[177] N. Wang, M. Chen, J. Gao, X. Ji, J. He, J. Zhang, W. Zhao, Talanta 195 (2019) 281–289.
[178] X. Wang, J. Cao, C. Zhao, Org. Biomol. Chem. 10 (2012) 4689–4691.
[179] F. Wang, G. Xu, X. Gu, Z. Wang, Z. Wang, B. Shi, C. Lu, X. Gong, C. Zhao, Biomaterials 159 (2018) 82–90.
[180] Y. Zhang, X. Shao, Y. Wang, F. Pan, R. Kang, F. Peng, Z. Huang, W. Zhang, W. Zhao, Chem. Commun. 51 (2015) 4245–4248.
[181] D. Lee, K. Jeong, X. Luo, G. Kim, Y. Yang, X. Chen, S. Kim, J. Yoon, J. Mater. Chem. B 6 (2018) 2541–2546.
[182] J. Gao, Y. Tao, N. Wang, J. He, J. Zhang, W. Zhao, Spectrochim. Acta A 203 (2018) 77–84.
[183] X. Sheng, D. Chen, M. Cao, Y. Zhang, X. Han, X. Chen, S. Liu, H. Chen, J. Yin, Chinese J. Chem. 34 (2016) 594–598.
[184] L. Wu, K. Burgess, Org. Lett. 10 (2008) 1779–1782.
[185] J. Liu, Y.-Q. Sun, H. Zhang, Y. Huo, Y. Shi, W. Guo, Chem. Sci. 5 (2014) 3183–3188.
[186] T.K. Chung, M.A. Funk, D.H. Baker, J. Nutr. 120 (1990) 158–165.
[187] Y.M. Go, D.P. Jones, Circulation 111 (2005) 2973–2980.
[188] J. Liu, M. Liu, H. Zhang, X. Wei, J. Wang, M. Xian, W. Guo, Chem. Sci. 10 (2019) 10065–10071.
[189] G. Xu, Q. Yan, X. Lv, Y. Zhu, K. Xin, B. Shi, R. Wang, J. Chen, W. Gao, P. Shi, C. Fan, C. Zhao, H. Tian, Angew. Chem. Int. Ed. 57 (2018) 3626–3630.
[190] Z. Qu, J. Ding, M. Zhao, P. Li, J. Photochem. Photobiol. A 299 (2015) 1–8.
[191] W. Chen, W.P. Bay, M.W. Wong, D. Huang, Tetrahedron Lett. 53 (2012) 3843–3846.
[192] Y. Men, Z. Li, J. Zhang, Z. Tong, Z. Xi, X. Qiu, L. Yi, Tetrahedron Lett. 56 (2015) 5781–5786.
[193] J. Pan, Y. Zhang, J. Xu, J. Liu, L. Zeng, G.-M. Bao, RSC Adv. 5 (2015) 97781–97787.
[194] J. Wang, H. Yu, Q. Li, S. Shao, Talanta 144 (2015) 763–768.
[195] Z. Zhu, W. Liu, L. Cheng, Z. Li, Z. Xi, L. Yi, Tetrahedron Lett. 56 (2015) 3909–3912.
[196] Y.L. Pak, J. Li, K.C. Ko, G. Kim, J.Y. Lee, J. Yoon, Anal. Chem. 88 (2016) 5476–5481.
[197] W. Chen, H. Luo, X. Liu, J.W. Foley, X. Song, Anal. Chem. 88 (2016) 3638–3646.
[198] P. Hou, H. Li, S. Chen, Tetrahedron 72 (2016) 3531–3534.
[199] Q. Hu, C. Yu, X. Xia, F. Zeng, S. Wu, Biosens. Bioelectron. 81 (2016) 341–348.
[200] L.A. Montoya, M.D. Pluth, Anal. Chem. 86 (2014) 6032–6039.
[201] D. Lee, G. Kim, J. Yin, J. Yoon, Chem. Commun. 51 (2015) 6518–6520.
[202] I. Ismail, Z. Chen, L. Sun, X. Ji, H. Ye, X. Kang, H. Huang, H. Song, S.G. Bolton, Z. Xi, M.D. Pluth, L. Yi, Chem. Sci. 11 (2020) 7823–7828.
[203] I. Ismail, D. Wang, Z. Wang, D. Wang, C. Zhang, L. Yi, Z. Xi, Dyes Pigments 163 (2019) 700–706.
[204] L. Sun, Y. Jiang, C. Zhang, X. Ji, D. Lv, Z. Xi, L. Yi, New J. Chem. 42 (2018) 15277–15283.
[205] P. Wang, Y. Wang, N. Li, J. Huang, Q. Wang, Y. Gu, Sens. Actuat. B 245 (2017) 297–304.
[206] H.-J. Xiang, H.P. Tham, M.D. Nguyen, S.Z. Fiona Phua, W.Q. Lim, J.-G. Liu, Y. Zhao, Chem. Commun. 53 (2017) 5220–5223.
[207] J. Xu, J. Pan, Y. Zhang, J. Liu, L. Zeng, X. Liu, Sens. Actuat. B 238 (2017) 58–65.
[208] X. Yang, L. He, K. Xu, W. Lin, Anal. Chim. Acta 981 (2017) 86–93.
[209] Z. Ye, C. Duan, Q. Hu, Y. Zhang, C. Qin, L. Zeng, J. Mater. Chem. B 5 (2017) 3600–3606.
[210] H. Niu, B. Ni, K. Chen, X. Yang, W. Cao, Y. Ye, Y. Zhao, Talanta 196 (2019) 145–152.
[211] L. Zhai, Z. Shi, Y. Tu, S. Pu, Dyes Pigments 165 (2019) 164–171.
[212] X. Gao, X. Li, L. Li, J. Zhou, H. Ma, Chem. Commun. 51 (2015) 9388–9390.
[213] S. Ding, W. Feng, G. Feng, Sens. Actuat. B 238 (2017) 619–625.
[214] L. He, X. Yang, K. Xu, X. Kong, W. Lin, Chem. Sci. 8 (2017) 6257–6265.
[215] H. Yu, Y. Liu, J. Wang, Q. Liang, H. Liu, J. Xu, S. Shao, New J. Chem. 41 (2017) 4416–4423.
[216] Y. Tang, G.-F. Jiang, New J. Chem. 41 (2017) 6769–6774.
[217] Y. Wang, X. Lv, W. Guo, Dyes Pigments 139 (2017) 482–486.
[218] X. Yang, C. Zhang, L. Shen, H. Bao, J. Xu, X. Fang, Y. Zhao, W. Yang, Sens. Actuat. B 242 (2017) 332–337.
[219] K. Zhang, J. Zhang, Z. Xi, L.Y. Li, X. Gu, Q.Z. Zhang, L. Yi, Chem. Sci. 8 (2017) 2776–2781.
[220] C. Zhang, Q.Z. Zhang, K. Zhang, L.Y. Li, M.D. Pluth, L. Yi, Z. Xi, Chem. Sci. 10 (2019) 1945–1952.
[221] X. Ji, M. Lv, F. Pan, J. Zhang, J. Wang, J. Wang, W. Zhao, Spectrochim. Acta A 206 (2019) 1–7.
[222] Q. Han, Z. Mou, H. Wang, X. Tang, Z. Dong, L. Wang, X. Dong, W. Liu, Anal. Chem. 88 (2016) 7206–7212.
[223] M. Gao, F. Yu, H. Chen, L. Chen, Anal. Chem. 87 (2015) 3631–3638.
[224] M. Gao, X. Zhang, Y. Wang, Q. Liu, F. Yu, Y. Huang, C. Ding, L. Chen, Anal. Chem. 91 (2019) 7774–7781.
[225] M. Gao, R. Wang, F. Yu, L. Chen, Biomaterials 160 (2018) 1–14.
[226] F. Yu, M. Gao, M. Li, L. Chen, Biomaterials 63 (2015) 93–101.
[227] X. Zhang, L. Zhang, M. Gao, Y. Wang, L. Chen, J. Hazard. Mater. 396 (2020) 122673.
[228] M. Gao, R. Wang, F. Yu, B. Li, L. Chen, J. Mater. Chem. B 6 (2018) 6637–6645.
[229] K. Yin, F. Yu, W. Zhang, L. Chen, Biosens. Bioelectron. 74 (2015) 156–164.
[230] C. Liu, W. Chen, W. Shi, B. Peng, Y. Zhao, H. Ma, M. Xian, J. Am. Chem. Soc. 136 (2014) 7257–7260.
[231] L. Yuan, W. Lin, Y. Xie, S. Zhu, S. Zhao, Chem.-Eur. J. 18 (2012) 14520–14526.
[232] X.F. Yang, Q. Huang, Y. Zhong, Z. Li, H. Li, M. Lowry, J.O. Escobedo, R.M. Strongin, Chem. Sci. 5 (2014) 2177–2183.
[233] M. Shimizu, H. Fukui, R. Shigitani, J. Chinese Chem. Soc. 63 (2016) 317–322.
[234] P. Dawson, T. Muir, I. Clark-Lewis, S. Kent, Science 266 (1994) 776–779.
[235] L. Long, W. Lin, B. Chen, W. Gao, L. Yuan, Chem. Commun. 47 (2011) 893–895.

[236] J.T. Rotruck, A.L. Pope, H.E. Ganther, A.B. Swanson, D.G. Hafeman, W.G. Hoekstra, Science 179 (1973) 588–590.
[237] J.W. Forstrom, J.J. Zakowski, A.L. Tappel, Biochemistry 17 (1978) 2639–2644.
[238] H. Sies, Free Radical Biol. Med. 14 (1993) 313–323.
[239] A. Muller, E. Cadenas, P. Graf, H. Sies, Biochem. Pharmacol. 33 (1984) 3235–3239.
[240] H. Sies, H. Masumoto, Adv. Pharmacol. 38 (1997) 229–246.
[241] B. Tang, Y. Xing, P. Li, N. Zhang, F. Yu, G. Yang, J. Am. Chem. Soc. 129 (2007) 11666–11667.
[242] R. Wang, L. Chen, P. Liu, Q. Zhang, Y. Wang, Chem.-Eur. J. 18 (2012) 11343–11349.
[243] H. Lv, X.-F. Yang, Y. Zhong, Y. Guo, Z. Li, H. Li, Anal. Chem. 86 (2014) 1800–1807.
[244] H. Zhang, L. Xu, W. Chen, J. Huang, C. Huang, J. Sheng, X. Song, ACS Sensors 3 (2018) 2513–2517.
[245] N. Wang, X. Ji, H. Wang, X. Wang, Y. Tao, W. Zhao, J. Zhang, Anal. Sci. (2020), https://doi.org/10.2116/analsci.20P134.
[246] Y. Men, X. Zhou, Z. Yan, L. Niu, Y. Luo, J. Wang, J. Wang, Anal. Sci. (2020), https://doi.org/10.2116/analsci.20P016.
[247] X.-L. Liu, L.-Y. Niu, Y.-Z. Chen, Y. Yang, Q.-Z. Yang, Biosens. Bioelectron. 90 (2017) 403–409.
[248] H. Zhang, L. Xu, W. Chen, J. Huang, C. Huang, J. Sheng, X. Song, Anal. Chem. 91 (2019) 1904–1911.
[249] S.Y. Lim, K.H. Hong, D.I. Kim, H. Kwon, H.J. Kim, J. Am. Chem. Soc. 136 (2014) 7018–7025.
[250] J. Yin, Y. Kwon, D. Kim, D. Lee, G. Kim, Y. Hu, J.H. Ryu, J. Yoon, J. Am. Chem. Soc. 136 (2014) 5351–5358.
[251] C. Dong, C.-Q. Zhou, J.-W. Yang, T.-C. Liao, J.-X. Chen, C.-X. Yin, W.-H. Chen, RSC Adv. 5 (2015) 32990–32993.
[252] J. Fan, Z. Han, Y. Kang, X. Peng, Sci. Rep. 6 (2016) 19562–19570.
[253] X. Liu, W. Zhang, C. Li, W. Zhou, Z. Li, M. Yu, L. Wei, RSC Adv. 5 (2015) 4941–4946.
[254] X. Zhu, Y. Li, W. Zan, J. Zhang, Z. Chen, X. Liu, F. Qi, X. Yao, X. Zhang, H. Zhang, Photochem. Photobiol. Sci. 15 (2016) 412–419.
[255] J. Lv, F. Wang, J. Qiang, X. Ren, Y. Chen, Z. Zhang, Y. Wang, W. Zhang, X. Chen, Biosens. Bioelectron. 87 (2017) 96–100.
[256] X.-B. Wang, D. Zhang, Sens. Actuat. B 241 (2017) 327–334.
[257] L. Xiong, J. Ma, Y. Huang, Z. Wang, Z. Lu, ACS Sensors 2 (2017) 599–605.
[258] J. Zhang, Z. Jin, X.X. Hu, H.M. Meng, J. Li, X.B. Zhang, H.W. Liu, T. Deng, S. Yao, L. Feng, Anal. Chem. 89 (2017) 8097–8103.
[259] R. Li, X. Huang, G. Lu, C. Feng, RSC Adv. 8 (2018) 24346–24354.
[260] F. Yu, P. Li, G. Li, G. Zhao, T. Chu, K. Han, J. Am. Chem. Soc. 133 (2011) 11030–11033.
[261] S.-R. Liu, S.-P. Wu, Org. Lett. 15 (2013) 878–881.
[262] Z. Guo, W. Zhu, L. Shen, H. Tian, Angew. Chem. Int. Ed. 46 (2007) 5549–5553.
[263] S.A. Hilderbrand, S.J. Lippard, Inorg. Chem. 43 (2004) 5294–5301.
[264] B. Biswal, B. Bag, Org. Biomol. Chem. 11 (2013) 4975–4992.
[265] J. Kim, S.-H. Lim, Y. Yoon, T.D. Thangadurai, S. Yoon, Tetrahedron Lett. 52 (2011) 2645–2648.
[266] P. Srivastava, R. Ali, S.S. Razi, M. Shahid, S. Patnaik, A. Misra, Tetrahedron Lett. 54 (2013) 3688–3693.
[267] Y. Pan, T.B. Ren, D. Cheng, Z.B. Zeng, L. Yuan, X.B. Zhang, Chem.-Asian J. 11 (2016) 3575–3582.
[268] Y. Huang, F. Yu, J. Wang, L. Chen, Anal. Chem. 88 (2016) 4122–4129.
[269] R. Wang, F. Yu, L. Chen, H. Chen, L. Wang, W. Zhang, Chem. Commun. 48 (2012) 11757–11759.
[270] M. Qian, L. Zhang, Z. Pu, J. Xia, L. Chen, Y. Xia, H. Cui, J. Wang, X. Peng, J. Mater. Chem. B 6 (2018) 7916–7925.
[271] L. Zhao, Q. Sun, C. Sun, C. Zhang, W. Duan, S. Gong, Z. Liu, J. Mater. Chem. B 6 (2018) 7015–7020.
[272] L. Zhang, X. Kai, Y. Zhang, Y. Zheng, Y. Xue, X. Yin, J. Zhao, Analyst 143 (2018) 4860–4869.
[273] J. Hong, Q. Xia, W. Feng, G. Feng, Dyes Pigments 159 (2018) 604–609.
[274] Y. Cheng, F. Ma, X. Gu, Z. Liu, X. Zhang, T. Xue, Y. Zheng, Z. Qi, Spectrochim. Acta A 210 (2019) 281–288.
[275] S. Chang, K. Xiang, W. Ming, X. Cheng, C. Han, Z. Zhang, B. Tian, J. Zhang, Res. Chem. Intermediat. 44 (2018) 5683–5695.
[276] J. Hong, W. Feng, G. Feng, Sens. Actuat. B 262 (2018) 837–844.
[277] K. Wang, C.-X. Zhao, T.-H. Leng, C.-Y. Wang, Y.-X. Lu, Y.-J. Shen, W.-H. Zhu, Dyes Pigments 151 (2018) 194–201.
[278] F. Huo, Y. Zhang, P. Ning, X. Meng, C. Yin, J. Mater. Chem. B 5 (2017) 2798–2803.
[279] X. Qiu, X. Jiao, C. Liu, D. Zheng, K. Huang, Q. Wang, S. He, L. Zhao, X. Zeng, Dyes Pigments 140 (2017) 212–221.
[280] X. Huang, H. Liu, J. Zhang, B. Xiao, F. Wu, Y. Zhang, Y. Tan, Y. Jiang, New J. Chem. 43 (2019) 6848–6855.
[281] Z. Du, B. Song, W. Zhang, C. Duan, Y.-L. Wang, C. Liu, R. Zhang, J. Yuan, Angew. Chem. Int. Ed. 130 (2018) 4063–4068.
[282] J. Kang, F. Huo, Y. Yao, C. Yin, Dyes Pigments 171 (2019) 107755–107760.
[283] Q. Zhao, F. Huo, Y. Zhang, Y. Wen, C. Yin, Spectrochim. Acta A 215 (2019) 297–302.
[284] K.P. Bhabak, G. Mugesh, Accounts Chem. Res. 43 (2010) 1408–1419.
[285] F. Wang, L. Zhou, C. Zhao, R. Wang, Q. Fei, S. Luo, Z. Guo, H. Tian, W.H. Zhu, Chem. Sci. 6 (2015) 2584–2589.
[286] X. Xie, M. Li, F. Tang, Y. Li, L. Zhang, X. Jiao, X. Wang, B. Tang, Anal. Chem. 89 (2017) 3015–3020.